Recursive Carrier Interferometry Aided High Data Rate OFDM Systems With PAPR Suppression, Phase Noise Rejection, and Carrier Frequency Offsets Compensation

Huaiyin Lu, Lin Zhang, *Senior Member, IEEE*, Xianyu Chen, and Zhiqiang Wu, *Senior Member, IEEE*

***Abstract*—In this paper, we propose two groups of recursive codes, namely the Hadamard recursive carrier interferometry (HRCI) codes and diagonal recursive carrier interferometry (DRCI) codes, to simultaneously reduce the peak-to-average power ratio (PAPR) and suppress the phase noises and residual carrier frequency offset (RCFO) for high-speed orthogonal frequency division multiplexing (OFDM) systems. We exploit the recursion property of the Hadamard and diagonal matrices to constitute the proposed HRCI code and DRCI code using the carrier interferometry (CI) code, and present the system model in details to spread OFDM symbols in the frequency domain. Then, we prove that both HRCI and DRCI generation matrices keep their invertibility during the recursions. As a direct result of the new code design, the phase intervals are enlarged and the signals are shifted in the time domain, thus both the PAPR and the phase noises are reduced, and the RCFO can be mitigated. Moreover, the enlarged phase intervals enable the transceiver blocks including the channel estimator, which estimate the phase noise based on the received signals, to improve the performance. Furthermore, we present the expressions for the HRCI and DRCI embedded transmitted and received signals, and derive the analytical signal-to-interference-plus-noise ratio (SINR) expressions for bit error rate (BER) performance analysis. Then, we analyze the effects of presented codes on the phase differences and provide the computational complexity analysis. Numerical simulations verify the effectiveness of our theoretical analysis of SINR. Additionally, under different parameter settings, which consider the working conditions of practical systems, we demonstrate that the presented robust HRCI and DRCI coded OFDM systems can suppress the PAPR satisfactorily and better BER performances can be achieved by the recursive CI-aided spread OFDM systems with phase noise rejection and RCFO compensation when compared with counterpart systems.**

***Index Terms*—Recursive carrier interferometry spreading code, hadamard recursion and diagonal recursion, peak to average power ratio, phase noise rejection, residual carrier frequency offset compensation.**

I. Introduction

In RECENT years, orthogonal frequency division multiplexing (OFDM) transmission technique has been widely used to meet the increasing demands for high data rate access to multimedia services. However, high speed OFDM transmissions will lead to higher peak to average power ratio (PAPR) of the transmitted OFDM signals and narrower sub-carrier phase intervals in a specified band. Additionally, OFDM systems will be more sensitive to carrier frequency drifting, thus degrading the performance of the wireless system.

A. Literature Review and Motivation

The spread orthogonal frequency division multiplexing (SOFDM) scheme has been proposed to enhance the performances of OFDM system over multipath fading channels by exploiting the diversity gain [1], with additional benefit of suppressing PAPR of the OFDM signals. In [2], a discrete fourier transform (DFT) scheme is presented for SOFDM systems, and the PAPR in DFT-SOFDM system can be suppressed for single carrier frequency division multiplexing access (SC-FDMA) systems. Then, the PAPR is further lowered by [3] and [4], which respectively propose to apply zero-tail DFT-SOFDM and unique word DFT-SOFDM to replace cyclic prefix for better tail characteristics to achieve better bit error rate (BER) performances in rich scattering environment. However, in DFT-SOFDM systems, some bands are used for transmitting the specified sequences to attain low PAPR [5], which results in bandwidth wastage and leads to a lower spectral efficiency. The carrier interferometry (CI) codes can be used as spreading codes in SOFDM systems to suppress PAPR with high spectral efficiency [6]–[8]. On one hand, the CI codes would not require to use additional sub-bands to transmit the specified sequences, and could spread OFDM symbols over all N sub-carriers to suppress PAPR, thus

Manuscript received May 4, 2018; revised September 12, 2018 and January 7, 2019; accepted February 8, 2019. Date of publication February 18, 2019; date of current version April 16, 2019. This work was supported in part by the National Natural Science Foundation of China under Grants 61602531 and 61572534, in part by the National Science Foundation under Grant 1323240, in part by the Office of Naval Research under Contract N00024-14-C-4073, and in part by the Opening Project of Guangdong Provincial Key Laboratory of Information Security Technology under Grant 2017B030314131. The review of this paper was coordinated by Dr. J.-C. Chen. *(Corresponding author: Lin Zhang.)*

H. Lu and L. Zhang are with the School of Electronics and Information Technology and the Guangdong Provincial Key Laboratory of Information Security Technology, Sun Yat-sen University, Guangzhou 510006, China (e-mail: 513284310@qq.com; isszl@mail.sysu.edu.cn).

X. Chen is with the School of Electronics and Information Technology, Sun Yat-sen University, Guangzhou 510006, China (e-mail: 734992689@qq.com).

Z. Wu is with the Department of Electrical Engineering, Tibet University, Lasa 850000, China, and also with the Wright State University, Dayton, OH 45435 USA (e-mail: zhiqiang.wu@wright.edu).

Digital Object Identifier 10.1109/TVT.2019.2900012

the spectral efficiency is attained without performance losses. On the other hand, compared with other spreading codes such as Hadamard-Walsh code [6], the CI spreading code can be designed in a more flexible way according to the number of sub-carriers of any integer value. Moreover, non-contiguous CI codes can be applied in dynamic spectrum access cognitive radio network [6] to eliminate the loss of orthogonality among spreading codes caused by deactivating sub-carriers. Thus with higher spectral utilization and spectral efficiency, the CI coded systems can achieve lower PAPR and better BER performances over frequency-selective fading channel [7] by suppressing the narrowband interferences [8].

However, high speed spread OFDM systems may suffer from smaller phase intervals between signals over different sub-carriers in the specified band and become more sensitive to carrier frequency drifting. In other words, when the sub-carrier number increases, the phase intervals would become smaller, which leads to the performance degradation in the presence of phase noise and residual carrier frequency offset (RCFO). Besides, as indicated by [15], since the impact of the phase noise can become even more profound when the systems operate at higher carrier frequencies, such as $E-band/70-80$ GHz, it is increasingly important to develop efficient detection algorithms for compensating the effect of the carrier frequency offset (CFO) and the phase noise in high data rate OFDM systems with the large bandwidth and densely spaced sub-carriers.

The phase noise is a random process caused by the fluctuation of the receiver and transmitter oscillators. In OFDM systems, phase noises will induce the loss of orthogonality between sub-carriers [9]. Pollet $et\,al.$ analytically evaluated the influence of CFO and the phase noise on the BER performance degradation for OFDM systems [9]. Then, Wu $et\,al.$ presented a general phase noise suppression scheme [10] and derived a closed-form expression for the signal-to-noise-plus-interference ratio (SINR) for exact performance analysis. Furthermore, in order to compensate the phase noises at OFDM receivers, Mathecken $et\,al.$ proposed phase noise estimation schemes that utilize the geometry associated with the spectral components of the complex exponential of phase noise [11], and [11] presented a new phase noise spectral model to evaluate the phase noise more exactly. Joint estimations of the channel response, the frequency offset, and the phase noise are also proposed for better estimations in realistic OFDM systems [12]–[15].

In addition, RCFO, which is caused by estimation errors of existing frequency offset recovery methods, will generate the phase drift over each sub-carrier and destroy the sub-carrier orthogonality [16]. [17] analyzed the effect of RCFO on performance degradations. Then, Sliskovic proposed a pilot-aided sampling and the carrier frequency offset estimator which derives the frequency estimates by comparing the phases of the pilots at the receiver side [18]. In addition, tracking possible RCFO variation during the data section of the frame is also helpful to improve the system performance and [19] proposed a new decision-directed synchronization scheme for carrier frequency offset estimations for OFDM systems.

B. Contributions

Different from existing phase noise rejection schemes[11]–[15] and RCFO compensation schemes [18], [19] for radio frequency (RF) systems, in this paper, we present recursive spreading CI code to simultaneously suppress PAPR and combat the phase noise as well as the RCFO for high speed OFDM systems over RF channels, thus both the reliability and the robustness of the system can be improved. In our previous work [20], we investigated the phase noise issue for optical OFDM systems. In this paper, we propose a generalized algorithm to construct the recursive CI codes to simultaneously suppress PAPR, reject the phase noises and compensate the carrier frequency offset for high speed RF OFDM systems.

The main contributions of this paper include:

1) Based on the recursion principle, we present Hadamard recursive CI (HRCI) codes and Diagonal recursive CI (DRCI) spreading codes in complex domain to enlarge the phase intervals between transmitted signals. With the enlarged phase intervals, the information transmission with densely spaced sub-carriers can accommodate phase noises and frequency offset variations to improve the reliability performances;
2) We prove that the invertibility properties of generation matrices constructed with Hadamard recursion and diagonal recursion are held during recursions. Accordingly, the inverse matrices of the presented HRCI and DRCI coding matrices are existent and can be used for information retrieval at the receiver;
3) Theoretical performance analysis is provided. We derive SINR expressions, then we compare the theoretical SINR of HRCI and DRCI aided systems with different parameter settings with the counterpart systems. Thanks to the enlarge phase intervals, the presented systems achieve better SINR performances, which can thereby improve the reliability performances.

Specifically, we propose a recursive spread code generation algorithm and two new recursive CI codes, which are called long HRCI and DRCI codes. Hadamard recursion is a general matrix extension process which realizes the extension of Hadamard matrices [21], and the resultant HRCI codes have multiple elements and their phases are different, which are different from conventional Hadamard matrices whose elements are 1 or -1. In addition, we apply diagonal recursion, which is a matrix extension process of calculating the Kronecker product of 2 order identity matrix and CI code matrix, and present DRCI codes. Then, we prove that both HRCI codes and DRCI codes inherit the benefits of conventional CI code, including the invertibility and orthogonality properties of the generation matrices during the recursion process.

Furthermore, we analytically derive the SINR expressions based on the phase noise model in [10] and the RCFO model in [16] to evaluate the performances of systems using our presented HRCI codes and DRCI codes. More specifically, we firstly derive the expression of demodulated signal based on these models. By separating the information-bearing signal and the interferences from the received data, we conduct an

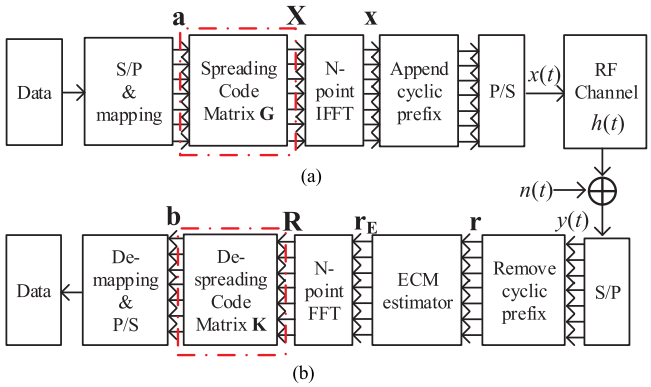

Fig. 1. SOFDM system.(S/P: serial to parallel; IFFT: inverse fast Fourier transform; P/S: parallel to serial; RF: radio frequency; ECM: expectation conditional maximization; FFT: discrete Fourier transform.)

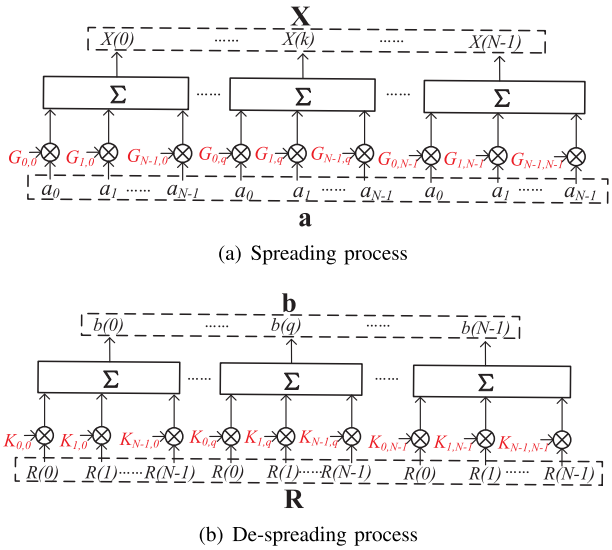

Fig. 2. Spreading process and de-spreading process of presented recursive CI codes aided SOFDM systems.

analytical analysis on the formulations of received signal. Then, the SINR expression can be obtained by calculating the average power of information-bearing signals and the interferences induced to the received data.

C. Paper Organization

The rest of the paper is organized as follows. We first introduce the SOFDM system model and the issues of phase noise and RCFO. Subsequently, in Section III we present the recursive spreading code design, and propose two novel types of Hadamard recursion and diagonal recursion based spreading CI codes. Besides, we provide the theoretical analysis of the characteristic of Hadamard recursion and diagonal recursion. In Section IV, we apply the proposed HRCI and DRCI codes to SOFDM systems and decompose the demodulated signal into the information-bearing signals and interferences. Then, we derive the corresponding SINR for the received data. Section V provides simulation results to verify the effectiveness of theoretical analysis, and to analyze the reliability, PAPR and the robustness performances for the presented HRCI and DRCI coded SOFDM systems. Finally we conclude our findings in Section VI.

II. Spreading OFDM System Model

In this section, we firstly describe the spreading OFDM system and present the issues of phase noise and CFO in detail. Subsequently, we provide the phase noise model, the CFO model, ECM estimator and the RCFO model as below. Then, the baseband signal model is derived.

A. System Model

Fig. 1 illustrates the block diagram of SOFDM system [6], [22]. At the transmitter side, after a serial-to-parallel (S/P) conversion, the data stream is mapped to data symbols. After spread by the codes expressed in terms of a $N \times N$ matrix $\mathbf{G}$, the data symbols are modulated by the N-point inverse fast Fourier transform (IFFT) module, wherein N denotes the sub-carrier number. After performing cyclic prefix extensions and parallel-to-serial (P/S) conversions, the SOFDM transmitters output the information-bearing signals $x(t)$ for transmission over RF channels.

At the receiver side, after removing the cyclic prefix in the received signal $\mathbf{r}$, we apply the expectation conditional maximization (ECM) estimator proposed in [15] to jointly estimate the channel state information, phase noise, and CFO in SOFDM systems. Thanks to the estimation of signal parameters, the equalizer is not required to be employed to mitigate the inter-symbol-interferences (ISI) as in [23]. Next, N-point fast Fourier transform (FFT) and the de-spreading code $N \times N$ matrix $\mathbf{K}$ are applied to the received signal to realize the de-spreading process. After de-mapping and the P/S conversion, the transmitted data can be recovered.

As illustrated in Fig. 1, at the transmitter, the spreading code matrix $\mathbf{G}$ is applied to data $\mathbf{a}$ and the details of the spreading process are given in Fig. 2(a). More specifically, we calculate the inner product of input data $\mathbf{a} = [a_0, a_1, \ldots, a_{N-1}]$ and each column of matrix $\mathbf{G}$ which is expressed as $\mathbf{X} = \mathbf{aG}$,

$$X(k) = \sum_{i=0}^{N-1} a_i \mathbf{G}_{i,k}. \tag{1}$$

Similarly, at the receiver, the de-spreading code matrix $\mathbf{K}$ is applied to the received signal to obtain the demodulated signal $\mathbf{b}$ and details of the de-spreading process $\mathbf{b} = \mathbf{RK}$ are provided in Fig. 2(b). The de-spreading process is expressed as

$$b(q) = \sum_{k=0}^{N-1} R(k) \mathbf{K}_{k,q}. \tag{2}$$

Subsequently, according to the definition of CI code given by [8]

$$\{\zeta_0^k, \zeta_1^k, \ldots, \zeta_{M-1}^k\} = \{e^{j\frac{2\pi}{M}\cdot k\cdot 0}, e^{j\frac{2\pi}{M}\cdot k\cdot 1}, \ldots, e^{j\frac{2\pi}{M}\cdot k\cdot (M-1)}\}, \tag{3}$$

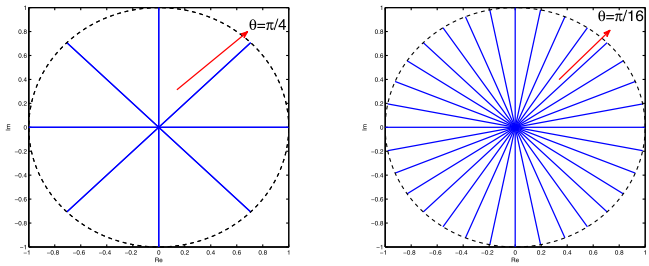

(a) M=8 (b) M=32

Fig. 3. Phase interval of CI codes for different M.

where k indicates the k^{th} symbol's spreading sequence characterized by $\{\zeta_0^k, \zeta_1^k, \ldots, \zeta_{M-1}^k\}$. We rewrite CI code in a matrix form and the $M \times M$ conventional spreading CI code matrix $\mathbf{G_{CI}}$ is defined as

$$\mathbf{G_{CI}}_{i,l} = exp\left(-j\frac{2\pi}{M} i * l\right), 0 \le i, l \le M-1, \quad (4)$$

where $j = \sqrt{-1}$, $\mathbf{G_{CI}}_{i,l}$ is the the element in i^{th} row and l^{th} column of matrix $\mathbf{G_{CI}}$ and conventional de-spreading CI code matrix $\mathbf{K_{CI}}$ is

$$\mathbf{K_{CI}}_{i,l} = exp\left(j\frac{2\pi}{M} i * l\right), 0 \le i, l \le M-1. \quad (5)$$

The relation between the sub-carrier number N and the dimension of $\mathbf{G_{CI}}$ and $\mathbf{K_{CI}}$ will be discussed in III-A. Besides, the details of the proposed recursive CI codes $\mathbf{G}$ and $\mathbf{K}$, which are respectively constituted by the CI spreading matrix $\mathbf{G_{CI}}$ and the CI de-spreading matrix $\mathbf{K_{CI}}$, will also be provided.

B. Phase Noise and CFO Issues for SOFDM Systems

In high speed SOFDM systems, in order to support high data rate transmissions, the sub-carrier number is required to be large, thus the length of the spreading code becomes longer and the phase intervals of signals over different sub-carriers become smaller. Thereby the SOFDM systems become more sensitive to phase noises and carrier frequency drifting.

To be more specific, the phase intervals between the elements of a $M \times M$ matrix $\mathbf{A}$ can be calculated by

$$\varphi = \min\left(\left|\arctan\left(\frac{\Im(\mathbf{A}_{i,l})}{\Re(\mathbf{A}_{i,l})}\right) - \arctan\left(\frac{\Im(\mathbf{A}_{i+1,l})}{\Re(\mathbf{A}_{i+1,l})}\right)\right|\right)$$
$$0 \le i \le M-2,\ 0 \le l \le M-1. \quad (6)$$

Take the code length of $M = 8$ and $M = 32$ as an example. As shown in Fig. 3, phase intervals are respectively $\pi/4$ and $\pi/16$ for the CI codes with length of $M = 8$ and $M = 32$, which proves that phase intervals among CI codes increase as the length of CI code decreases.

Due to the smaller phase interval among CI codes, large scale CI code based SOFDM systems are more sensitive to phase noise than those without CI code. In addition, the CFO generates the phase drift in each sub-carrier and destroys the sub-carrier orthogonality, which causes a even worse situation when the phase intervals become smaller.

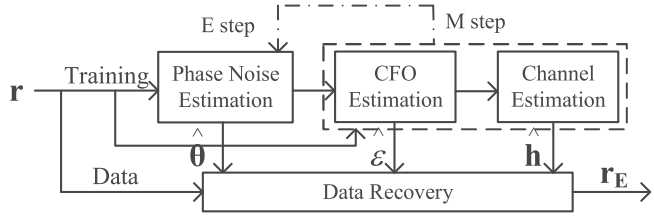

Fig. 4. ECM Estimator.

Next, we provide the phase noise model, the CFO model and the baseband signal model.

C. Phase Noise and CFO Model

Phase noise θ, which occurs at both transmitter and receiver oscillators, can be presented as a finite-power Wiener process which has independent Gaussian increments [24]–[27]. In this paper, the phase noise model developed by Demir [28], which provides more accurate descriptions by using a nonlinear method, is used to characterize the phase noise as

$$\theta_n = \theta_{n-1} + \zeta_n,\ n = 1, \ldots N, \quad (7)$$

where θ_n denotes the phase noise at the n^{th} instant, $\zeta_n \sim N(0, \sigma_\zeta^2)$ is the phase noise innovation, $\sigma_\zeta^2 = 2\pi\beta T/N$ is the variance of the innovation process, β denotes the phase noise linewidth, T is the symbol period in OFDM system, N is the sub-carrier number, and $R = N/T$ denotes the transmission data rate.

On the other hand, the normalized CFO $\epsilon = \Delta f T$ is modeled as a uniformly distributed random variable over the range $\epsilon \in (-0.5, 0.5)$ [12], [29]. The CFO vector $\mathbf{E}$ is defined as

$$E(n) = e^{(j2\pi n\epsilon/N)},\ n = 0, 1, \ldots, N-1, \quad (8)$$

where $E(n)$ is the n^{th} element of $\mathbf{E}$ and represents the frequency offset of the n^{th} sub-carrier.

D. ECM Estimator and RCFO Model

In this paper, the ECM estimator proposed in [15] is applied on the received signals, which realizes the joint estimation of the channel state, the phase noise, and CFO in SOFDM systems. The ECM based estimation is carried out in two steps. In the expectation step (E-step), an extended Kalman filter (EKF) based estimator is utilized to accurately track the phase noise in the training OFDM symbol. During the maximization step (M-step), the channel state and CFO parameters are estimated by minimizing the derived negative log likelihood function.

More specifically, as shown in Fig. 4, the ECM algorithm iterates between the E-step and the M-step [15]. In the E-step, an EKF is used to update the phase noise vector at the $(i+1)^{th}$ iteration with the aid of the estimated channel state and CFO at the i^{th} iteration shown by the dotted arrow in Fig. 4. Next, in the M-step, the estimates of the channel state and CFO at the $(i+1)^{th}$ iteration are obtained. The ECM algorithm iteratively updates the phase noise, CFO, and channel state estimates, respectively. Subsequently, the algorithm is terminated when the difference between the likelihood functions of two iterations is

smaller than a threshold η given by

$$\left| \sum_{n=0}^{N-1} \left\| r(n) - e^{\frac{j2\pi n \hat{\epsilon}^{[i+1]}}{N}} e^{j\hat{\theta}^{[i+1]}(n)} s^{[i+1]}(n) \right\|^2 - \sum_{n=0}^{N-1} \left\| r(n) - e^{\frac{j2\pi n \hat{\epsilon}^{[i]}}{N}} e^{j\hat{\theta}^{[i]}(n)} s^{[i]}(n) \right\|^2 \right| \leq \eta, \tag{9}$$

where $\hat{\epsilon}^{[i+1]}$ and $\hat{\theta}^{[i+1]}$ are the estimates of CFO and phase noise at the $(i+1)^{th}$ iteration respectively. More specifically, the $s^{[i]}(n)$ is the n^{th} symbol of the vector $\mathbf{s}^{[i]} \triangleq \mathbf{F_I X V \hat{h}}^{[i]}$ where $\mathbf{F_I}$ is the $N \times N$ inverse discrete fourier transform (IDFT) matrix, $\mathbf{V}$ is the $N \times L$ discrete fourier transform (DFT) matrix, L indicates the number of channel taps and $\hat{\mathbf{h}}^{[i]}$ is the estimate of channel state at the i^{th} iteration. Finally, after algorithm is terminated, the estimates of channel state $\hat{\mathbf{h}}$, CFO $\hat{\epsilon}$ and phase noise $\hat{\theta}$ are used for data recovery.

As illustrated in [15], with the aid of the ECM estimator, more reliable communication can be achieved with a low computation complexity. However, the impact of the channel state, the phase noise and CFO cannot be completely eliminated. In the following descriptions, we use the channel spectral response $\mathbf{H}'$, the new phase noise ϕ and RCFO to represent the residue values of the channel state, the phase noise and CFO after ECM estimations.

More explicitly, the residue phase noise ϕ is characterize as

$$\phi_n = \phi_{n-1} + \delta_n,\ n = 1, \ldots N, \tag{10}$$

where ϕ_n denotes the phase noise at the n^{th} instant, $\delta_n \sim N(0, \sigma_\delta^2)$ is the phase noise innovation, and we have $\sigma_\delta^2 < \sigma_\zeta^2$ with the aid of the ECM estimator.

Subsequently, as to the RCFO, considering that the uniform random CFO estimation and the compensation are applied at receiver [15], [29], [30], we here regard the RCFO as a Gaussian random variable [30]

$$\nu \sim N(0, \sigma_\nu^2), \tag{11}$$

where ν is the Gaussian random variable that describes RCFO and σ_ν^2 is the variance of ν.

E. Baseband Signal Model

As illustrated in Fig. 1, IFFT operations are performed on signals $\{X(k)\}_{k=0}^{N-1}$ over N sub-carriers in the frequency domain to produce the corresponding N modulated signals in the time domain. The baseband signal can be expressed as

$$x(n) = \frac{1}{\sqrt{N}} \sum_{k=0}^{N-1} X(k) e^{\frac{j2\pi n k}{N}}. \tag{12}$$

At receiver, after the cyclic prefix removal, the received signal $\mathbf{r}$ is

$$r(n) = e^{j\theta(n)}[x(n) * \mathcal{F}^{-1}(H(k))] + z(n), \tag{13}$$

where $*$ and $\mathcal{F}^{-1}(.)$ represent the circular convolution and IFFT operations, respectively, while $z(n)$ indicates the additive white Gaussian noise (AWGN) with zero mean and variance σ^2. $H(k)$ is the frequency domain channel response which is determined by a specific channel. After ECM estimation process and N-point FFT, with the aid of received signal expression in [10], take the RCFO signal model of [16], [17] into consideration, we have the expression of $\mathbf{R}$ as

$$R(k) = X(k)H'(k)\Upsilon_1(k) + \Upsilon_2(k) + Z(k), \tag{14}$$

where $\Upsilon_1(k)$ denotes fading and phase shift of the transmitted signal caused by the phase noise and RCFO, $\Upsilon_2(k)$ is the interference caused by phase noise and RCFO, $Z(k)$ is AWGN in the frequency domain after FFT process. Since FFT does not change the noise energy, $Z(k)$ is still a Gaussian random variable with zero mean and variance σ^2. The expression of $\Upsilon_1(k)$ is

$$\Upsilon_1(k) = I(0) e^{j2\pi N_B k \nu_k / N} f_N(\nu_k), \tag{15}$$

and $\Upsilon_2(k)$ is expressed as

$$\Upsilon_2(k) = ICI(k) e^{j2\pi N_B k \nu_k / N} f_N(\nu_k). \tag{16}$$

In equations (15) and (16), $e^{j2\pi N_B k \nu_k / N} f_N(\nu_k)$ denotes fading and phase shift cause by RCFO. More explicitly, let ν_k denote the RCFO of the k^{th} sub-carrier and $N_B = N + N_g$ denote the length of the time domain transmitted signals, thus we have

$$f_N(x) = e^{j\pi x(N-1)/N} \frac{\sin(\pi x)}{N \sin(\pi x / N)}. \tag{17}$$

In addition, the items $e^{j\pi\nu_k[2N_B k + (N-1)]/N}$ and $\frac{\sin(\pi\nu_k)}{N\sin(\pi\nu_k/N)}$ in (15) and (17) represent the phase rotations and amplitude variations brought by the RCFO respectively. In equations (15), $I(0)$ represents the effects of common phase error (CPE) caused by phase noise. Moreover, $I(p)$ is defined as [10]

$$I(p) = \frac{1}{N} \sum_{n=0}^{N-1} e^{j[\frac{2\pi p n}{N} + \phi(n)]}, \tag{18}$$

In equations (16), $ICI(k) = \Sigma_{l=0, l\neq k}^{N-1} X(l)H'(l)I(l-k)$ is inter-carrier-interference (ICI) cause by phase noise.

At last, the expression of $\Upsilon_1(k)$ and $\Upsilon_2(k)$ can be further derived as

$$\Upsilon_1(k) = \frac{1}{N} \sum_{n=0}^{N-1} \frac{\sin(\pi\nu_k)}{N\sin(\pi\nu_k/N)} e^{j\{\pi\nu_k[2N_B k + (N-1)]/N + \phi(n)\}} \tag{19}$$

$$\Upsilon_2(k) = \frac{1}{N} \sum_{n=0}^{N-1} \sum_{l=0, l\neq k}^{N-1} X(l)H'(l) \frac{\sin(\pi\nu_k)}{N sin(\pi\nu_k/N)} \cdot e^{j\{\pi[2(l-k)n + 2N_B k\nu_k + (N-1)\nu_k]/N + \phi(n)\}}. \tag{20}$$

III. Recursive HRCI Code and DRCI Code Design

In order to combat the phase noises and the RCFO presented above, in this section, we firstly present the recursive spreading CI code design, then, we give the construction details of HRCI codes and DRCI codes. Moreover, we analyze the properties of the recursive code generation matrices to investigate whether the presented spreading codes can be applied in SOFDM systems.

Algorithm 1: Recursive Spread Code Generation.

1: **Initialisation:** Obtain k in (21), CI code matrices $\mathbf{G_{CI}}$, $\mathbf{K_{CI}}$ and recursion type $\mathbf{TYPE} = 'Hadamard'$ $or\,'diagonal'$. Set $i = 1$ for $\mathbf{TYPE} = 'Hadamard'$, $i = 0$ for $\mathbf{TYPE} = 'diagonal'$, spreading matrix $\mathbf{G} = \mathbf{G_{CI}}$, de-spreading matrix $\mathbf{K} = \mathbf{K_{CI}}$, $n = 0$.
2: **repeat**
3: Kronecker product extension matrix $\mathbf{W} = \left(\frac{1}{\sqrt{2}}\begin{bmatrix} 1 & 1 \\ 1 & -1 \end{bmatrix}\right)^i$
4: Recursion for spreading matrix $\mathbf{G} = \mathbf{W} \otimes \mathbf{G}$.
5: Recursion for de-spreading matrix $\mathbf{K} = \mathbf{W} \otimes \mathbf{K}$.
6: $n = n + 1$
7: **until** $n = k$.
8: **return** $\mathbf{G}$ for spreading matrix and $\mathbf{K}$ for de-spreading matrix

A. Recursive Spreading CI Code Design

We here propose to construct long spreading code with short codes via recursions. Let M denote the dimension of spreading code matrix, which is determined according to the number of sub-carriers denoted by N, namely we have

$$N = 2^k M,\ 0 \leq k, \tag{21}$$

where k is selected to satisfy that N can be divided by 2^k.

Algorithm 1 describes the procedure of generating recursion-based spreading codes, and the Kronecker product [31] extension matrix for extending the code matrices is determined by the recursion type.

More explicitly, in Hadamard recursion process, $i = 1$ and Kronecker product extension matrix is $\mathbf{W} = \frac{1}{\sqrt{2}}\left[\begin{smallmatrix} 1 & 1 \\ 1 & -1 \end{smallmatrix}\right]$ which can realize Hadamard recursion for generating HRCI code. When another type of the diagonal recursion is applied, $i = 0$ and Kronecker product extension matrix is denoted by $\mathbf{W} = \left[\begin{smallmatrix} 1 & 0 \\ 0 & 1 \end{smallmatrix}\right]$ which is the same as Eq. (28) and utilizes the diagonal recursion to generate the DRCI codes.

It is worth pointing out that the presented DRCI code and HRCI code inherit the PAPR suppression capabilities from traditional CI codes [6] which utilizes the complex exponential elements of CI codes to address the PAPR issue caused by IFFT. Note that the CI code matrix is essentially a FFT matrix, employing a full rank CI code to cancel the IFFT and therefore provides a signal with the same PAPR as a single carrier transmission. Similar technologies such as the single carrier FDMA (SC-FDMA) and the single carrier transmission with the frequency domain equalization have been proposed and developed to reduce the PAPR of multi-carrier transmissions. In the proposed schemes in this manuscript, the DRCI code and HRCI code do not eliminate the PAPR entirely like a full rank CI code, but it does reduce the PAPR significantly through inheritance of the PAPR suppression characteristic of traditional CI code.

Moreover, the presented DRCI code and HRCI code maintain the relatively larger phase intervals of short CI codes. To be more explicit, in Algorithm 1, after carrying out the logical OR operation of the normalized matrix $\mathbf{W} = \frac{1}{\sqrt{2}}\left[\begin{smallmatrix} 1 & 1 \\ 1 & -1 \end{smallmatrix}\right]$ and the identity matrix, i.e., $\mathbf{W} = \frac{1}{\sqrt{2}}\left[\begin{smallmatrix} 1 & 1 \\ 1 & -1 \end{smallmatrix}\right] \bigvee \left[\begin{smallmatrix} 1 & 0 \\ 0 & 1 \end{smallmatrix}\right]$ where $\bigvee$ represents the logical OR operation, the value of the elements in the resultant matrix are typically $\{-1, 0, 1\}$. That is to say, Algorithm 1 recursively generates HRCI codes and DRCI codes using the elements in the matrices $\mathbf{G_{CI}}$ and $\mathbf{K_{CI}}$, thus the phase intervals of resultant DRCI codes and HRCI codes are the same as those of short CI code matrices $\mathbf{G_{CI}}$ and $\mathbf{K_{CI}}$.

Thus, thanks to enlarged phase intervals, the presented DRCI code and HRCI code can combat the phase noises and the CFO, thus they have the capability of the phase noise rejection and the RCFO mitigation while effectively suppressing the PAPR.

Take $k = 2$ and $N = 4M$ as an example. The details of the corresponding spreading and de-spreading code design based on Algorithm 1 is given as below.

B. Hadamard Recursion and HRCI Code Design

It is well known that high order Hadamard matrix can be generated from a low order one by Hadamard recursion [21]. Assuming $\mathbf{H}$ is a Hadamard matrix of order n, Hadamard recursion is defined as

$$\mathbf{H_{2n}} = \begin{bmatrix} \mathbf{H} & \mathbf{H} \\ \mathbf{H} & -\mathbf{H} \end{bmatrix}, \tag{22}$$

where $\mathbf{H_{2n}}$ is a Hadamard matrix of order $2n$.

Using the CI code given by (4), we propose to generate the HRCI codes according to Algorithm 1 in the following way

$$\mathbf{G_{2M,H}} = \begin{bmatrix} \mathbf{G_{CI}} & \mathbf{G_{CI}} \\ \mathbf{G_{CI}} & -\mathbf{G_{CI}} \end{bmatrix},$$
$$\mathbf{G_{4M,H}} = \begin{bmatrix} \mathbf{G_{2M,H}} & \mathbf{G_{2M,H}} \\ \mathbf{G_{2M,H}} & -\mathbf{G_{2M,H}} \end{bmatrix}. \tag{23}$$

After the normalization, the HRCI spreading code matrix $\mathbf{G_H}$ is expressed as

$$\mathbf{G_H} = \frac{1}{\sqrt{N}}\mathbf{G_{4M,H}}. \tag{24}$$

Similarly, the de-spreading code matrix can be generated through

$$\mathbf{K_{2M,H}} = \begin{bmatrix} \mathbf{K_{CI}} & \mathbf{K_{CI}} \\ \mathbf{K_{CI}} & -\mathbf{K_{CI}} \end{bmatrix}, \mathbf{K_{4M,H}} = \begin{bmatrix} \mathbf{K_{2M,H}} & \mathbf{K_{2M,H}} \\ \mathbf{K_{2M,H}} & -\mathbf{K_{2M,H}} \end{bmatrix}, \tag{25}$$

and the HRCI de-spreading code matrix $\mathbf{K_H}$ is

$$\mathbf{K_H} = \frac{1}{\sqrt{N}}\mathbf{K_{4M,H}}. \tag{26}$$

C. Diagonal Recursion and DRCI Code Design

Similar to the Hadamard recursion, the diagonal recursion can also be applied to generate high order matrix from a low order one and hold the matrix invertibility property.

Assuming $\mathbf{D}$ is a square matrix of order n, the definition of diagonal recursion is

$$\mathbf{D_{2n}} = \begin{bmatrix} \mathbf{D} & \mathbf{0_n} \\ \mathbf{0_n} & \mathbf{D} \end{bmatrix}, \tag{27}$$

where $\mathbf{D_{2n}}$ is a high order matrix of order $2n$. More explicitly, the diagonal recursion process can be realized by calculating the Kronecker product [31] of a 2-order identity matrix and a low order matrix as

$$\mathbf{D_{2n}} = \begin{bmatrix} 1 & 0 \\ 0 & 1 \end{bmatrix} \otimes \mathbf{D} = \begin{bmatrix} \mathbf{D} & \mathbf{0_n} \\ \mathbf{0_n} & \mathbf{D} \end{bmatrix}, \tag{28}$$

where $\otimes$ indicates Kronecker product.

Utilizing diagonal recursion in (27) and CI code in (4), the spreading code matrix can be generated through

$$\mathbf{G_{2M,D}} = \begin{bmatrix} \mathbf{G_{CI}} & \mathbf{0_M} \\ \mathbf{0_M} & \mathbf{G_{CI}} \end{bmatrix}, \mathbf{G_{4M,D}} = \begin{bmatrix} \mathbf{G_{2M,D}} & \mathbf{0_{2M}} \\ \mathbf{0_{2M}} & \mathbf{G_{2M,D}} \end{bmatrix}. \tag{29}$$

After the normalization, the DRCI spreading code matrix $\mathbf{G_D}$ is expressed as

$$\mathbf{G_D} = \frac{1}{\sqrt{M}} \mathbf{G_{4M,D}}. \tag{30}$$

Similarly, the de-spreading code matrix can be generated through

$$\mathbf{K_{2M,D}} = \begin{bmatrix} \mathbf{K_{CI}} & \mathbf{0_M} \\ \mathbf{0_M} & \mathbf{K_{CI}} \end{bmatrix}, \mathbf{K_{4M,D}} = \begin{bmatrix} \mathbf{K_{2M,D}} & \mathbf{0_{2M}} \\ \mathbf{0_{2M}} & \mathbf{K_{2M,D}} \end{bmatrix}, \tag{31}$$

and the DRCI de-spreading code matrix $\mathbf{K_D}$ is

$$\mathbf{K_D} = \frac{1}{\sqrt{M}} \mathbf{K_{4M,D}}. \tag{32}$$

D. Invertibility Property Analysis for Recursive Spreading Carrier Interferometry Codes

Considering that the invertibility of the spreading code matrix is required in SOFDM system for de-spreading when recovering the received data, we will prove that the invertibility property is held during both Hadamard recursion and Diagonal recursion as follows.

Theorem 1: Matrix invertibility property is held during the Hadamard recursion.

Proof: Assuming $\mathbf{Z}$ is an n order nonsingular matrix, we have $\mathbf{Z^{-1}Z} = \mathbf{I_n}$ where $\mathbf{Z^{-1}}$ is the inverse matrix of $\mathbf{Z}$ and $\mathbf{I_n}$ is an n order identity matrix. The zero elements in $\mathbf{I_n}$ can be calculated by

$$(\mathbf{Z^{-1}Z})_{i,j,\, i \neq j} = \sum_{k=1, i \neq j}^{n} \mathbf{Z}^{-1}_{i,k} \mathbf{Z}_{k,j} = 0. \tag{33}$$

Utilizing (23), a high order matrix of $2n$ generated by Hadamard recursion from $\mathbf{Z}$ can be expressed as

$$\mathbf{Y} = \begin{bmatrix} \mathbf{Z} & \mathbf{Z} \\ \mathbf{Z} & -\mathbf{Z} \end{bmatrix}, \tag{34}$$

$$\mathbf{Y}_{i,j} = \begin{cases} \mathbf{Z}_{i,j}, & 1 \le i \le n, 1 \le j \le n \\ \mathbf{Z}_{i,j-n}, & 1 \le i \le n, n+1 \le j \le 2n \\ \mathbf{Z}_{i-n,j}, & n+1 \le i \le 2n, 1 \le j \le n \\ -\mathbf{Z}_{i-n,j-n}, & n+1 \le i \le 2n, n+1 \le j \le 2n \end{cases}. \tag{35}$$

Similarly, applying Hadamard recursion, $\mathbf{Z^{-1}}$ can be extended as

$$\mathbf{P} = \begin{bmatrix} \mathbf{Z^{-1}} & \mathbf{Z^{-1}} \\ \mathbf{Z^{-1}} & -\mathbf{Z^{-1}} \end{bmatrix}. \tag{36}$$

As for $1 \le i \le n, 1 \le j \le n$, utilizing (33) and (35), the result of $\mathbf{PY}$ is

$$\begin{aligned} (\mathbf{PY})_{i,j} &= \sum_{k=1}^{2n} \mathbf{P}_{i,k} \mathbf{Y}_{k,j} = \sum_{k=1}^{n} \mathbf{P}_{i,k} \mathbf{Y}_{k,j} + \sum_{k=n+1}^{2n} \mathbf{P}_{i,k} \mathbf{Y}_{k,j} \\ &= \sum_{k=1}^{n} \mathbf{Z}^{-1}_{i,k} \mathbf{Z}_{k,j} + \sum_{k=1}^{n} \mathbf{Z}^{-1}_{i,k} \mathbf{Z}_{k,j} \\ &\Rightarrow \mathbf{PY} = 2\mathbf{I_n},\ 1 \le i \le n, 1 \le j \le n. \end{aligned} \tag{37}$$

Similarly, we have

$$(\mathbf{PY})_{i,j} = \begin{cases} \mathbf{0_n}, & 1 \le i \le n, n+1 \le j \le 2n \\ \mathbf{0_n}, & n+1 \le i \le 2n, 1 \le j \le n \\ 2\mathbf{I_n}, & n+1 \le i \le 2n, n+1 \le j \le 2n \end{cases}, \tag{38}$$

where $\mathbf{0_n}$ is an order n zero matrix. Thus, we have

$$\mathbf{PY} = 2\mathbf{I_{2n}}, \tag{39}$$

where $\mathbf{I_{2n}}$ is a $2n$ order identity matrix.

Taking the normalization factor $1/\sqrt{2}$ in Algorithm 1 into consideration, we can come to a conclusion from (39) that $\mathbf{P}$ is the inverse matrix of $\mathbf{Y}$ and matrix inverse property is held during Hadamard recursion. The proof is completed. ■

Theorem 2: Matrix inverse property is held during diagonal recursion.

Proof: Assuming $\mathbf{D}$ is a n order nonsingular matrix, we have $\mathbf{D^{-1}D} = \mathbf{I_n}$ where $\mathbf{D^{-1}}$ is the inverse matrix of $\mathbf{D}$ and $\mathbf{I_n}$ is an order n identity matrix. The zero elements in $\mathbf{I_n}$ can be calculated by

$$(\mathbf{D^T D})_{i,j,\, i \neq j} = \sum_{k=1, i \neq j}^{n} \mathbf{D}_{k,i} \mathbf{D}_{k,j} = 0. \tag{40}$$

According to (27), the element of $\mathbf{D_{2n}}$ can be expressed as

$$(\mathbf{D_{2n}})_{i,j} = \begin{cases} \mathbf{D}_{i,j}, & 1 \le i \le n, 1 \le j \le n \\ 0, & 1 \le i \le n, n+1 \le j \le 2n \\ 0, & n+1 \le i \le 2n, 1 \le j \le n \\ \mathbf{D}_{i-n,j-n}, & n+1 \le i \le 2n, n+1 \le j \le 2n \end{cases}. \tag{41}$$

Applying the diagonal recursion, a high order matrix generated from $\mathbf{D^{-1}}$ can be extended as

$$\mathbf{Q} = \begin{bmatrix} \mathbf{D^{-1}} & \mathbf{0_n} \\ \mathbf{0_n} & \mathbf{D^{-1}} \end{bmatrix}. \tag{42}$$

Similar to (37) and (38), we have

$$(\mathbf{QD_{2n}})_{i,j} = \begin{cases} \mathbf{I_n}, & 1 \le i \le n, n+1 \le j \le 2n \\ \mathbf{0_n}, & 1 \le i \le n, n+1 \le j \le 2n \\ \mathbf{0_n}, & n+1 \le i \le 2n, 1 \le j \le n \\ \mathbf{I_n}, & n+1 \le i \le 2n, n+1 \le j \le 2n \end{cases}. \tag{43}$$

Thus, we have the similar result as (39)

$$\mathbf{QD_{2n}} = \mathbf{I_{2n}}, \tag{44}$$

which indicates $\mathbf{Q}$ is the inverse matrix of $\mathbf{D_{2n}}$ and the matrix invertibility property is held during diagonal recursions. The proof is completed. ■

E. The Effects of Recursive Spreading CI Codes on Phase Differences

The analysis of the effects of recursive spreading CI codes on phase differences is presented in this subsection. As illustrated in Fig. 1 and Fig. 2, the spreading code matrix $\mathbf{G}$ is applied to input data, then we investigate the effects of the joint spreading process and IFFT on the phase difference, which are expressed as the multiplication of the spreading code matrix $\mathbf{G}$ and the $N \times N$ IDFT matrix $\mathbf{F_I}$.

1) DRCI Code: Utilizing equation (21) and Algorithm 1, we get an $N \times N$ DRCI code matrix $\mathbf{G_D}$ constituted from multiple short CI coding matrices $\mathbf{G_{CI}}$ which have a number of 2^k and are sequentially generated at the main diagonal line as

$$\mathbf{G_D} = \frac{1}{\sqrt{M}} \underbrace{\begin{bmatrix} \mathbf{G_{CI}} & & \\ & \ddots & \\ & & \mathbf{G_{CI}} \end{bmatrix}}_{2^k}, \tag{45}$$

where $\mathbf{G_{CI}}$ is the short CI code matrix of the dimension M defined in (4).

Subsequently, the effects of the joint spreading process and IFFT are expressed as the multiplication of the DRCI coding matrix $\mathbf{G_D}$ and the $N \times N$ IDFT matrix $\mathbf{F_I}$

$$\mathbf{S} = \mathbf{G_D F_I} = \frac{1}{\sqrt{M}} \begin{bmatrix} \mathbf{G_{CI}} & & \\ & \ddots & \\ & & \mathbf{G_{CI}} \end{bmatrix}$$

$$\mathbf{F_I} = \begin{bmatrix} \mathbf{S_0} & & \\ & \ddots & \\ & & \mathbf{S_{2^k-1}} \end{bmatrix}. \tag{46}$$

To be more explicit, the expression of the t^{th} submatrix $\mathbf{S_t}, 0 \le t \le 2^k - 1$ of the matrix $\mathbf{S}$ is

$$\begin{aligned} \mathbf{S_t}_{(a,b)} &= \frac{1}{\sqrt{M}} \sum_{i=0}^{M-1} e^{-j\frac{2\pi}{M}ai} e^{j\frac{2\pi}{N}(i+tM)(b+tM)} \\ &= \frac{1}{\sqrt{M}} \frac{1 - e^{j2\pi\frac{b+tM}{2^k}}}{1 - e^{j\frac{2\pi}{M}[\frac{b+tM}{2^k} - a]}} e^{j\frac{2\pi}{N}btM + t^2M^2}, \\ & 0 \le a, b \le M-1, \end{aligned} \tag{47}$$

where $\mathbf{S_t}_{(a,b)}$ represents the element in the a^{th} row and the b^{th} column of the matrix $\mathbf{S_t}$.

Accordingly, the phase difference between the elements of matrix S_t is obtained as

$$\begin{aligned} \Phi_{\mathbf{S_t}} &= \left| angle(\mathbf{S_t}_{(a+1,b)}) - angle(\mathbf{S_t}_{(a,b)}) \right|, \\ & 0 \le a \le M-2,\ 0 \le b \le M-1. \end{aligned} \tag{48}$$

2) HRCI Code: Utilizing equation (21) and Algorithm 1, we can obtain an $N \times N$ HRCI coding matrix $\mathbf{G_H}$ generated by the Hadamard recursion as given by equation (22). Since there are more nonzero elements in the matrix, the analysis of the effects of HRCI codes is more complicated. Here we take $k = 1$ and N = 2M as an example. The expression of $\mathbf{G_H}$ is

$$\mathbf{G_H} = \frac{1}{\sqrt{N}} \begin{bmatrix} \mathbf{G_{CI}} & \mathbf{G_{CI}} \\ \mathbf{G_{CI}} & -\mathbf{G_{CI}} \end{bmatrix} \tag{49}$$

Then the effect of joint spreading process and IFFT on the phase difference is given by

$$\mathbf{U} = \mathbf{G_H F_I} = \frac{1}{\sqrt{N}} \begin{bmatrix} \mathbf{G_{CI}} & \mathbf{G_{CI}} \\ \mathbf{G_{CI}} & -\mathbf{G_{CI}} \end{bmatrix} \mathbf{F_I} = \begin{bmatrix} \mathbf{L} & \mathbf{Q} \\ \mathbf{Q}^H & \mathbf{T} \end{bmatrix}. \tag{50}$$

Since $\mathbf{G_H}$ and $\mathbf{F_I}$ are unitary matrices, the matrix $\mathbf{U}$ is also a unitary matrix.

To be more explicit, the expression of the submatrices of the matrix $\mathbf{U}$ is given by

$$\begin{aligned}\mathbf{L}_{(a,b)} &= \frac{1}{\sqrt{N}}\left[\sum_{i=0}^{M-1} e^{-j\frac{2\pi}{M}ai}e^{j\frac{2\pi}{N}ib} + \sum_{i=0}^{M-1} e^{-j\frac{2\pi}{M}ai}e^{j\frac{2\pi}{N}(i+M)b}\right] \\ &= \frac{1}{\sqrt{N}}\frac{1-e^{j2\pi\frac{b}{2^k}}}{1-e^{j\frac{2\pi}{M}[\frac{b}{2^k}-a]}}(1+e^{j2\pi\frac{b}{2^k}}), 0 \le a,b \le M-1,\end{aligned} \tag{51}$$

$$\begin{aligned}\mathbf{Q}_{(a,b)} &= \frac{1}{\sqrt{N}}\left[\sum_{i=0}^{M-1} e^{-j\frac{2\pi}{M}ai}e^{j\frac{2\pi}{N}i(b+M)} + \sum_{i=0}^{M-1} e^{-j\frac{2\pi}{M}ai}e^{j\frac{2\pi}{N}(i+M)(b+M)}\right] \\ &= \frac{1}{\sqrt{N}}\frac{1-e^{j2\pi\frac{b+M}{2^k}}}{1-e^{j\frac{2\pi}{M}[\frac{b+M}{2^k}-a]}}(1+e^{j2\pi\frac{b+M}{2^k}}), \\ &0 \le a,b \le M-1,\end{aligned} \tag{52}$$

$$\begin{aligned}\mathbf{T}_{(a,b)} &= \frac{1}{\sqrt{N}}\left[\sum_{i=0}^{M-1} e^{-j\frac{2\pi}{M}ai}e^{j\frac{2\pi}{N}i(b+M)} - \sum_{i=0}^{M-1} e^{-j\frac{2\pi}{M}ai}e^{j\frac{2\pi}{N}(i+M)(b+M)}\right] \\ &= \frac{1}{\sqrt{N}}\frac{1-e^{j2\pi\frac{b+M}{2^k}}}{1-e^{j\frac{2\pi}{M}[\frac{b+M}{2^k}-a]}}(1-e^{j2\pi\frac{b+M}{2^k}}), \\ &0 \le a,b \le M-1.\end{aligned} \tag{53}$$

Accordingly, the phase difference between the elements of matrix U is obtained as

$$\begin{aligned}&\Phi = \left|angle(\mathbf{U}_{(a+1,b)}) - angle(\mathbf{U}_{(a,b)})\right|, \\ &0 \le a \le M-2,\ 0 \le b \le M-1.\end{aligned} \tag{54}$$

With the aid of the expressions presented above, we can further investigate and compare the PAPR and the phase interval performances between the preposed system and the counterpart system via simulations in Section. V.

F. Computational Complexity Analysis for Recursive Spreading CI Codes

In this subsection, the computational complexity of recursive spreading CI codes is compared with that of conventional CI code and reference [12], [15]. Moreover, the comparison of the computational complexity of SOFDM and OFDM is provided.

1) Code Generation: Firstly, as illustrated in Section II-B conventional CI codes of length N are generated through equation (4) and (5) whose computational complexity are $O(N^2)$.

Secondly, short CI codes $\mathbf{G_{CI}}$ of the length M are generated through equation (4) and equation (5) whose computational complexity is $O(M^2)$. Subsequently, the recursive spreading code generation process illustrated in Algorithm 1 is expressed as

$$\mathbf{G} = \underbrace{\mathbf{W}\otimes\mathbf{W}\otimes\ldots\otimes\mathbf{W}}_{k}\underbrace{\otimes\mathbf{G_{CI}}}_{\diamondsuit}. \tag{55}$$

More explicitly, the computational complexity of calculating Kronecker product is determined by the size of the product matrix which can be expressed as

$$\mathbf{C} = \mathbf{A}\otimes\mathbf{B}, Size(\mathbf{C}) = (N,M) \Longrightarrow Com = MN. \tag{56}$$

Therefore, computational complexity of recursive spreading CI codes generation is

$$\begin{aligned}Com_{RCI} &= N^2 + \left(\frac{N}{2}\right)^2 + \ldots + \underbrace{\left(\frac{N}{2^{k-1}}\right)^2}_{\diamondsuit} + \underbrace{M^2}_{\mathbf{G_{CI}}} \\ &= \frac{N^2(4-4^{1-k})}{3} = O(N^2),\end{aligned} \tag{57}$$

which is in the same order as conventional long CI codes.

2) SOFDM Spreading Process: The computational complexities induced by the spreading and the de-spreading operations in SOFDM systems in Fig. 1 are naturally determined by the complexity of the matrix multiplication of the $N \times N$ matrix and the $N \times 1$ vector which is $Com_{SOFDM} = O(N^2)$.

3) Comparison: The computational complexity of the estimation and data detection algorithms in reference [12], [15] are given by

$$\begin{aligned}Com_{[12],E} &= [22N^3 + 5N^2 - 3N - 1]t_{[12]} \\ &\quad + 18N^3 + (8L-5)N^2 - (2L+1)N - L,\end{aligned} \tag{58}$$

$$\begin{aligned}Com_{[15],E} &= [2N^3 + (12L+2)N^2 + (2L+25)N \\ &\quad + 1 - 2L]t_{[15],E} + 2N^3 + (2L-2)N^2 - LN,\end{aligned} \tag{59}$$

$$\begin{aligned}Com_{[15],D} &= [4N^4 + 4N^3 + (2L+1)N^2 + (L+13)N]t_{[15],D} \\ &\quad + 4N^4 + 3N^3 + (2L-1)N,\end{aligned} \tag{60}$$

where L indicates the number of channel taps, $t_{[12]}$ is the number of iterations required for estimating the CFO via an exhaustive search in [12], $t_{[15],E}$ is the number of iterations in the ECM estimator and $t_{[15],D}$ is the number of iterations required by the detector in [15].

Since the number of iterations is much smaller than N in both simulations and practical systems, the complexities of equations (58)–(60) can be expressed as $O(N^3), O(N^3), O(N^4)$ respectively. The complexities of proposed HRCI and DRCI codes in the SOFDM scheme and algorithms given by the reference [12] and [15] are summarized in Table I. More specifically, utilizing equation (57), the complexity of proposed HRCI and DRCI code in SOFDM scheme is $O(N^2)$, which is much lower than the ECM estimator (59) as well as the estimation and data detection algorithms presented in reference [12] and [15].

Additionally, we provide the complexity comparison between proposed recursive CI codes and the algorithm in [15] at different SNRs in Fig. 5. It can be seen from Fig. 5 that the proposed

TABLE I
COMPLEXITY COMPARISON

Algorithm	Code	Estimation	Detection	Total
[12]	—	$O(N^3)$	—	$O(N^3)$
[15]	—	$O(N^3)$	$O(N^4)$	$O(N^4)$
HRCI	$O(N^2)$	$O(N^3)$	—	$O(N^3)$
DRCI	$O(N^2)$	$O(N^3)$	—	$O(N^3)$

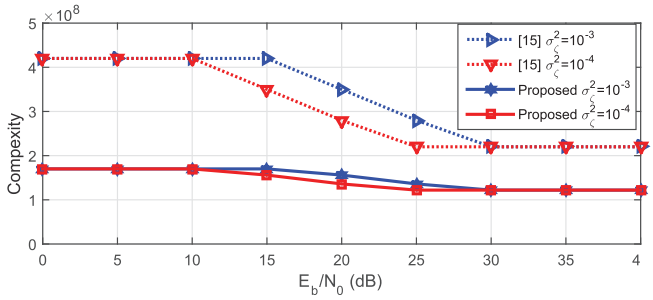

Fig. 5. Comparison of the computational complexity of the DRCI code, HRCI code and the algorithms in [15], N = 64, L = 4.

recursive CI codes are computationally more efficient compared to the algorithms in [15] at all SNRs.

IV. THEORETICAL PERFORMANCE ANALYSIS

In this section, we firstly describe the spread and de-spread signal based on the system model given in Section II-A and the recursive spreading code design presented in Section III, then, we analyze the SINR of SOFDM systems.

A. Spread and De-Spread Signal

As illustrated in Fig. 1 and Fig. 2, at the transmitter, the spreading code matrix $\mathbf{G}$ is applied to data $\mathbf{a}$, while at the receiver, the de-spreading code matrix $\mathbf{K}$ is applied to the received signal to obtain demodulated signal $\mathbf{b}$.

Substituting (14) into (1) and (2), the demodulated signal is obtained as

$$\begin{aligned} b(q) &= \frac{1}{N}\sum_{k=0}^{N-1}\sum_{i=0}^{N-1} a_i \mathbf{G}_{i,k}\mathbf{K}_{k,q}H'(k)\Upsilon_1(k) \\ &+ \frac{1}{\sqrt{N}}\sum_{k=0}^{N-1} Z(k)\mathbf{K}_{k,q} \\ &+ \frac{1}{N}\sum_{k=0}^{N-1}\sum_{i=0}^{N-1}\sum_{l=0,l\neq k}^{N-1} a_i \mathbf{G}_{i,l}\mathbf{K}_{k,q}H'(l) \\ &\times I(l-k)e^{j2\pi N_B k\nu_k/N} f_N(\nu_k). \end{aligned} \tag{61}$$

B. SINR Analysis

It can be seen from (61) that the demodulated signal $b(q)$ is constituted by the information-bearing signal, which contains a_q, and the interferences. Thus the first term of (61) becomes

$$\begin{aligned} &\frac{1}{N}\sum_{k=0}^{N-1}\sum_{i=0}^{N-1} a_i \mathbf{G}_{i,k}\mathbf{K}_{k,q}H'(k)\Upsilon_1(k) \\ &= \frac{1}{N}\sum_{k=0}^{N-1}\sum_{i=0,i\neq q}^{N-1} a_i \mathbf{G}_{i,k}\mathbf{K}_{k,q}H'(k)\Upsilon_1(k) \\ &+ \frac{1}{N}\sum_{k=0}^{N-1} a_q \mathbf{G}_{q,k}\mathbf{K}_{k,q}H'(k)\Upsilon_1(k), \end{aligned} \tag{62}$$

and the third term is

$$\begin{aligned} &\frac{1}{N}\sum_{k=0}^{N-1}\sum_{i=0}^{N-1}\sum_{l=0,l\neq k}^{N-1} a_i \mathbf{G}_{i,l}\mathbf{K}_{k,q}H'(l)I(l-k) \\ &\times e^{j2\pi N_B k\nu_k/N} f_N(\nu_k) \\ &= \frac{1}{N}\sum_{k=0}^{N-1}\sum_{i=0,i\neq q}^{N-1}\sum_{l=0,l\neq k}^{N-1} a_i \mathbf{G}_{i,l}\mathbf{K}_{k,q}H'(l)I(l-k) \\ &\times e^{j2\pi N_B k\nu_k/N} f_N(\nu_k) \\ &+ \frac{1}{N}\sum_{k=0}^{N-1}\sum_{l=0,l\neq k}^{N-1} a_q \mathbf{G}_{q,l}\mathbf{K}_{k,q}H'(l)I(l-k) \\ &\times e^{j2\pi N_B k\nu_k/N} f_N(\nu_k). \end{aligned} \tag{63}$$

Therefore, $\mathbf{b}$ can be expressed as

$$\begin{aligned} b(q) &= \frac{a_q}{N}\sum_{k=0}^{N-1}[\mathbf{G}_{q,k}\mathbf{K}_{k,q}H'(k)I(0) \\ &+ \sum_{l=0,l\neq k}^{N-1}\mathbf{G}_{q,l}\mathbf{K}_{k,q}H'(l)I(l-k)]e^{j2\pi N_B k\nu_k/N} f_N(\nu_k) \\ &+ \frac{1}{N}\sum_{k=0}^{N-1}\sum_{i=0,i\neq q}^{N-1}[a_i \mathbf{G}_{i,k}\mathbf{K}_{k,q}H'(k)I(0) \\ &+ \sum_{l=0,l\neq k}^{N-1} a_i \mathbf{G}_{i,l}\mathbf{K}_{k,q}H'(l)I(l-k)]e^{j2\pi N_B k\nu_k/N} f_N(\nu_k) \\ &+ \frac{1}{\sqrt{N}}\sum_{k=0}^{N-1} Z(k)\mathbf{K}_{k,q} \\ &= b_d(q)+b_i(q)+Z_n(q), \end{aligned} \tag{64}$$

where the information-bearing signal are the terms that contain a_q

$$\begin{aligned} b_d(q) &= \frac{a_q}{N}\sum_{k=0}^{N-1}[\mathbf{G}_{q,k}\mathbf{K}_{k,q}H'(k)I(0) \\ &+ \sum_{l=0,l\neq k}^{N-1}\mathbf{G}_{q,l}\mathbf{K}_{k,q}H'(l)I(l-k)]e^{j2\pi N_B k\nu_k/N} f_N(\nu_k). \end{aligned} \tag{65}$$

The second term of (65) can be derived as

$$\frac{a_q}{N}\sum_{k=0}^{N-1}\sum_{l=0,l\neq k}^{N-1}\mathbf{G}_{q,l}\mathbf{K}_{k,q}H'(l)I(l-k)e^{j2\pi N_B k\nu_k/N}f_N(\nu_k)$$
$$=\frac{a_q}{N}\sum_{k=0}^{N-1}\left[\sum_{l=0}^{N-1}\mathbf{G}_{q,l}\mathbf{K}_{k,q}H'(l)I(l-k)-\underbrace{\mathbf{G}_{q,k}\mathbf{K}_{k,q}H'(k)I(0)}_{l=k}\right]e^{j2\pi N_B k\nu_k/N}f_N(\nu_k). \quad (66)$$

Obviously, the second term in (66) is the same as the first term of (65) and therefore the expression of information-bearing signal is simplified as

$$b_d(q)=\frac{a_q}{N}\sum_{k=0}^{N-1}\sum_{l=0}^{N-1}\mathbf{G}_{q,l}\mathbf{K}_{k,q}H'(l)I(l-k)\times e^{j2\pi N_B k\nu_k/N}f_N(\nu_k). \quad (67)$$

Similarly, the interference in (64) is represented as

$$b_i(q)=\frac{1}{N}\sum_{k=0}^{N-1}\sum_{i=0,i\neq q}^{N-1}\left[a_i\mathbf{G}_{i,k}\mathbf{K}_{k,q}H'(k)I(0)+\sum_{l=0,l\neq k}^{N-1}a_i\mathbf{G}_{i,l}\mathbf{K}_{k,q}H'(l)I(l-k)\right]e^{j2\pi N_B k\nu_k/N}f_N(\nu_k). \quad (68)$$

and the corresponding simplified form is expressed as

$$b_i(q)=\frac{1}{N}\sum_{k=0}^{N-1}\sum_{i=0,i\neq q}^{N-1}\sum_{l=0}^{N-1}a_i\mathbf{G}_{i,l}\mathbf{K}_{k,q}H'(l)\cdot I(l-k)e^{j2\pi N_B k\nu_k/N}f_N(\nu_k). \quad (69)$$

Since the de-spreading matrices are normalized as illustrated in (26) and (32), the de-spreading process does not change signal energy and $Z_n(q)$ has the same properties as $Z(k)$.

Therefore, the SINR expression of SOFDM system is obtained as

$$\Gamma=\frac{E[|b_d(q)|^2]}{E[|b_i(q)|^2]+\sigma^2}. \quad (70)$$

where $E[|b_i(q)|^2]$ and $E[|b_d(q)|^2]$ respectively represent the signal and interference energy, which are derived in detail in Appendix. From the energy evaluation expressions given by Eq.(A6) and Eq.(A7), we can see that the system performances are dependent on the spreading codes employed, the phase noise variances and the statistic of RCFO.

V. Performance Analysis and Simulations

In this section, the performances of the proposed HRCI codes and DRCI codes aided SOFDM systems in the presence of phase noise and CFO are evaluated, and the performances of conventional CI code aided SOFDM systems are also provided as a reference. For performance comparison, we set the same parameters as in reference [15]. The main simulation parameters are summarized in Table II. More explicitly, the unknown normalized CFO is assumed to be uniformly distributed over range $\epsilon\in(-0.5,0.5)$ for each simulation and the data symbols are drawn from normalized 64 quadrature amplitude modulation (QAM).

TABLE II
Simulation Parameters

Parameters	Value
Modulation order	64QAM
Channel fading	Rayleigh
Channel taps	L=4
Channel taps power	[-1.52,-6.75,-11.91,-17.08]dB
Phase noise variance	$\sigma_\zeta^2=[10^{-3},10^{-4}]rad^2$
CFO	U(-0.5,0.5)
Sampling rate	20MHz

We firstly simulate the BER performances of SOFDM systems using different spreading codes over frequency selective Rayleigh fading channel under different phase noise variance and compare them with existing algorithms in the references [12], [15], [32], [33]. Then, we analyze the corresponding SINR performance. Subsequently, BER performance of different spreading codes aided SOFDM systems with different lengths of short CI codes are provided. Next, the comparisons of the phase interval for CI code, HRCI and DRCI codes with different code length is provided. Subsequently, the phase differences between the adjacent elements of the DRCI coding matrix, the HRCI coding matrix and IFFT transformation matrix are simulated. Finally, we analyze the PAPR performances of the SOFDM systems using the presented recursion based spreading codes and compare them with the counterpart system given in [34].

In the simulations, as mentioned above, the phase noise, CFO model and ECM estimator are employed. Besides, we here assume RCFO is a Gaussian random process as given in (11).

A. Performances of SOFDM Systems at Different Phase Noise Variance

1) BER Comparison With Existing Work at Different Phase Noise: Firstly, we simulate the BER performances of SOFDM systems using different spreading codes over Rayleigh channel under different phase noise variance and compare them with existing algorithms. The following system setups are considered for comparison:

i) The proposed HRCI code and DRCI code with ECM estimator in [15] (labelled as "HRCI" and "DRCI").
ii) The estimation and data detection algorithm in [15] (labelled as "[15]").
iii) The estimation and data detection algorithm in [12] and [32], respectively (labelled as "[12] & [32]").
iv) The differential chaotic shift keying (DCSK) design with CI code [33] (labelled as "[33]").
v) The conventional CI code(labelled as "CI").

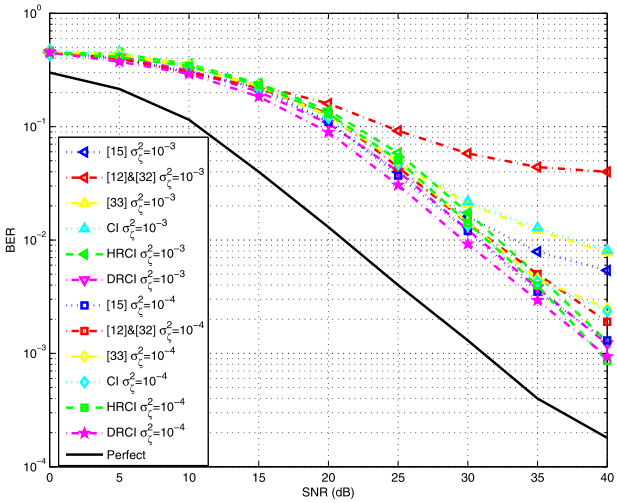

Fig. 6. Simulated BER performances of existing algorithm and SOFDM systems using CI, HRCI and DRCI codes over frequency selective Rayleigh fading channels with phase noises of different variances. The length of low order CI codes is $M = 16$.

vi) As a lower-bound on the BER performance, a system assuming perfect channel, phase noise, and CFO estimation (labelled as"Perfect").

Fig. 6 depicts the BER performance listed above. The following observations can be made from Fig. 6:

1) Compared to existing algorithms in [15], in the presence of the strong phase noise ($\sigma_\zeta^2 = 10^{-3}, R = 10^8, \beta = 1.59 * 10^4$), which is more representative of reality, the BER performances of the proposed HRCI and DRCI codes are closer to the ideal case of perfect channel estimation, phase noise, and CFO estimation (a performance gap of 6 dB at $SNR = 40$ dB), which indicates that the proposed HRCI and DRCI codes perform better than the data detection algorithm in [15]. On the other hand, the proposed HRCI and DRCI codes provide similar performances to the data detection algorithm in [15] in the presence of weak phase noise ($\sigma_\zeta^2 = 10^{-4} rad^2, R = 10^8, \beta = 1.59 * 10^3$).
2) It can be clearly observed that the proposed HRCI and DRCI codes outperform the algorithms in [12] and [32]. This performance improvement can be attributed to the fact that Algorithm 1 maintains the phase interval of the short CI code matrix and provide same phase noise robustness as short CI code. Moreover, the ECM estimator proposed in [15] also provides better estimation with the aid of EKF.
3) The existing algorithms in [33], which proposed DCSK design with CI code, provides similar BER performance to conventional CI code. It is clear that the performance of the proposed HRCI and DRCI codes outperform the algorithm in [33] and conventional CI code. This result is anticipated since Algorithm 1 maintains the phase interval of the short CI code matrix and provide the same phase noise robustness as short CI code. More explicitly, as illustrated in Fig. 3, the phase interval of the short CI code is larger than long CI code.

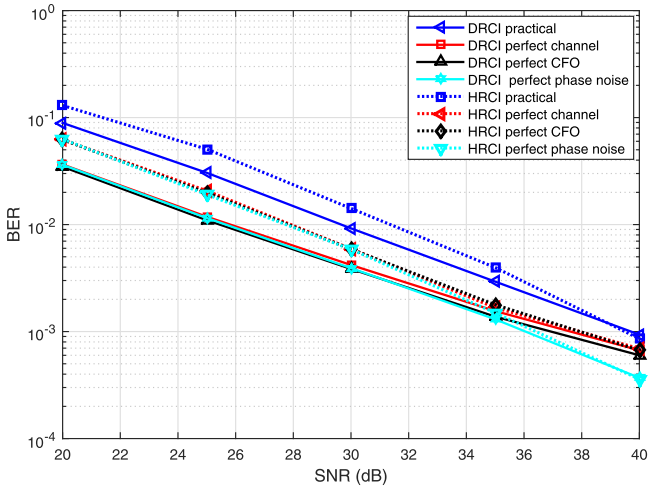

Fig. 7. BER performances of SOFDM systems using HRCI and DRCI codes under different parameter settings with perfect estimates. $M = 16$ $\sigma_\zeta^2 = 10^{-4} rad^2$.

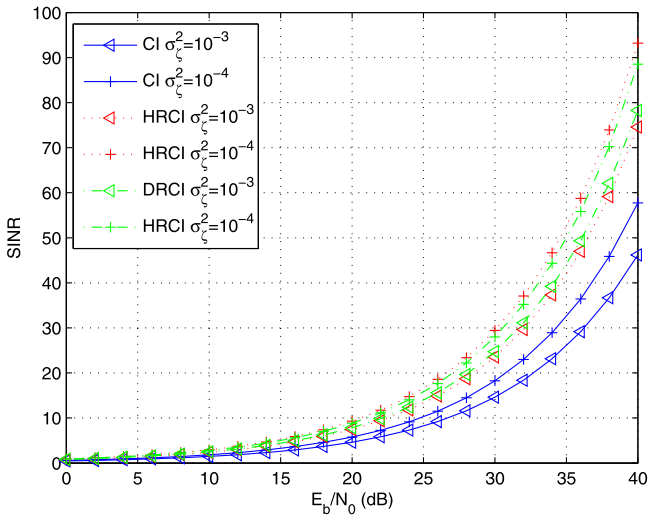

Fig. 8. SINR performances of SOFDM systems using CI, HRCI and DRCI codes over frequency selective Rayleigh fading channels with phase noises of different variances. The length of low order CI codes is $M = 16$.

2) Comparison of Effects of the Channel Conditions, Phase Noise, and Frequency Offset Estimations: Next, we investigate the effects of the channel, phase noise and frequency offset estimations on the BER performances. Specifically, under the assumptions of perfect channel estimation, perfect CFO estimation and perfect phase noise estimation, Fig. 7 compares the BER performances of SOFDM systems using HRCI and DRCI codes with different parameter settings. It can be observed that when the phase noise estimation is perfect, the BER performances are better than those obtained with perfect channel estimation and perfect CFO estimation.

3) SINR Performances: Subsequently, the SINR performances of SOFDM system with different spreading codes are calculated by equation (70) and compared in Fig. 8. From equation (61), we can see that the expression of $b(q)$ changes with the specific combination of information signal $\mathbf{a}$. Hence we here

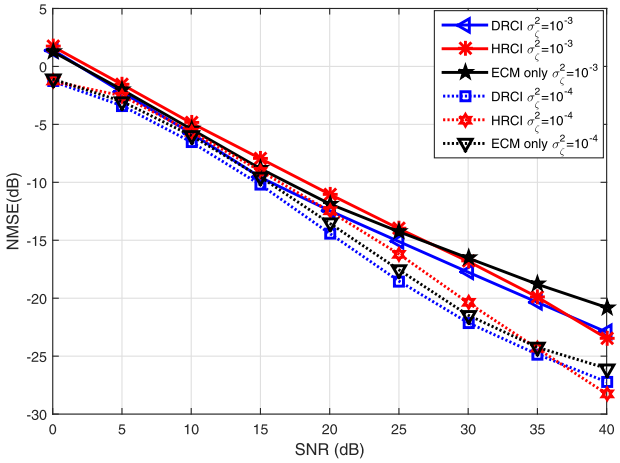

Fig. 9. NMSE performances of SOFDM systems using the ECM estimator with and without HRCI and DRCI codes. The length of low order CI codes is $M = 16$.

simulate the SINR of the recursion-based CI coded SOFDM systems by calculating more than 10^7 transmitted frames, which provides an approximative mean value of SINR. The SINR performances in Fig. 8 show the same result as BER performances in Fig. 6, which proves better robustness can be achieved by using our HRCI and DRCI codes.

4) NMSE Performances:

$$NMSE_{ECM} = 10\log_{10}\frac{\sum_{i=0}^{N-1}[r_E(i)-x(i)]^2}{\sum_{i=0}^{N-1}[x(i)]^2} \tag{71a}$$

$$NMSE_{Code} = 10\log_{10}\frac{\sum_{i=0}^{N-1}[b(i)-a(i)]^2}{\sum_{i=0}^{N-1}[a(i)]^2} \tag{71b}$$

Next, Fig. 9 compares the normalized mean square error (NMSE) performances of SOFDM systems using the ECM estimator with and without HRCI and DRCI codes, where the NMSE performances are evaluated by equation (71). To be more explicit, equations (71a) and (71b) can be respectively used to evaluate the NMSE of SOFDM systems using the ECM estimator without and with the recursive carrier interferometry code. It can be observed that in the presence of strong phase noise ($\sigma_\zeta^2 = 10^{-3} rad^2$), the NMSE performances of DRCI code aided systems are better than the systems only using the ECM estimator at all SNRs, while the systems using HRCI codes outperform those only using the ECM estimator at high SNR($SNR > 25dB$). The reason is that from equations (45)–(53), we can see that the nonzero elements in the matrix $\mathbf{Q}$ in equation (52), which is the submatrix used to evaluate the effects of the joint spreading process and IFFT $\mathbf{U}$, lead to the worse performances of SOFDM systems using HRCI codes at low SNR, while providing better performances than the systems using DRCI codes at high SNR thanks to more phase variations generated by the matrix $\mathbf{U}$. Besides, in the presence of weak phase noises ($\sigma_\zeta^2 = 10^{-4} rad^2$), we can attain similar results since the effects of channel state, CFO and phase noise on the NMSE performances can be further eliminated. Moreover, it is noticeable that better robustness can be achieved by using our HRCI and DRCI codes under the same phase noise and CFO circumstances.

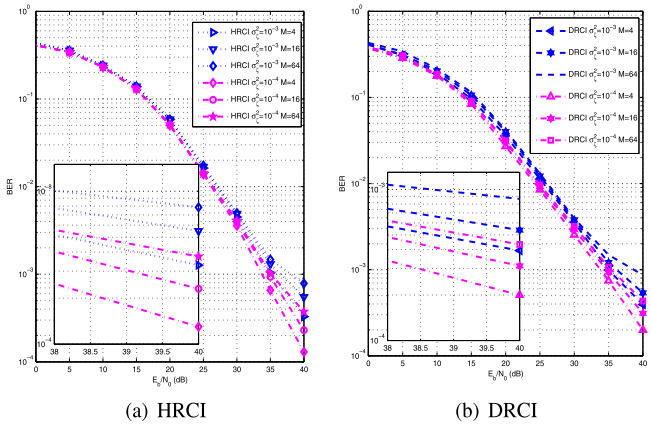

(a) HRCI (b) DRCI

Fig. 10. BER performances of SOFDM systems using the proposed HRCI and DRCI codes over frequency selective Rayleigh fading channels at different size of short CI codes.

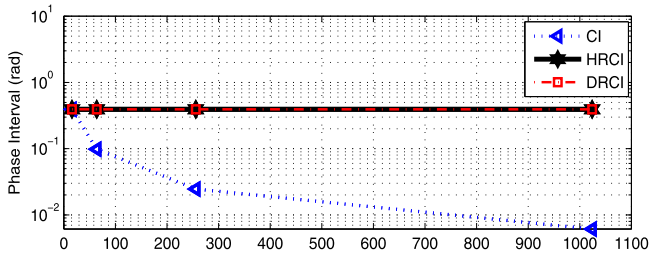

Fig. 11. Phase intervals of CI code, HRCI and DRCI codes with different N. $M = 16$.

B. Performance at Different Size of Short CI Codes

Subsequently, we analyze the BER performances of SOFDM systems using HRCI and DRCI codes with different length of low order CI code $M = 4, 16, 64$, wherein the phase noise variance are set to $\sigma_\zeta^2 = [10^{-3}, 10^{-4}] rad^2$. As shown in Fig. 10, both HRCI and DRCI coded SOFDM systems achieve better performances when using shorter length low order CI code since the shorter length low order CI code has lager phase interval as illustrated in Section II-B and thus providing better noise tolerance. In addition, from Fig. 10, we can also observe that the HRCI coded system achieves similar BER performances to those of DRCI coded SOFDM systems with different length of low order CI code.

Next, Fig. 11 illustrates the comparison of phase interval defined in (6) for CI code, HRCI and DRCI codes with different code length N. It can be observed that the phase intervals of HRCI and DRCI codes remain the same as N increases, while those of CI codes decrease with the increasing N. The reason is that thanks to the generation process in Algorithm 1, the phase intervals of HRCI and DRCI codes are determined by the short CI code, thereby bringing the noise-resistant performance benefits to the SOFDM systems.

In addition, utilizing the expressions which evaluate the phase differences given by equations (45)–(54), we simulate the phase

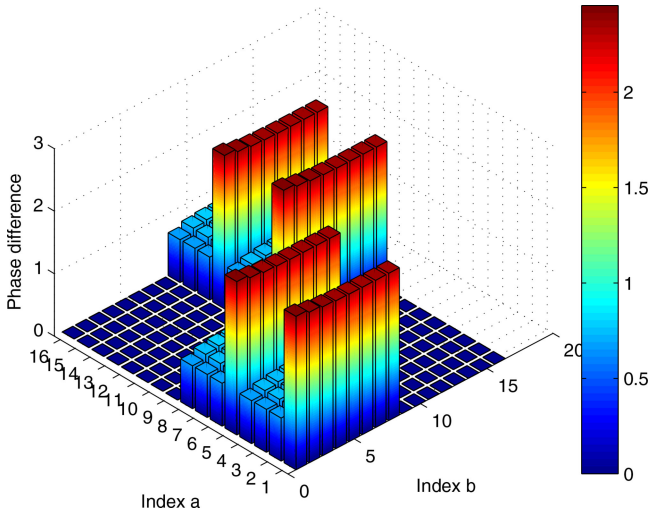

Fig. 12. Phase difference of DRCI code with $N = 16, M = 8$.

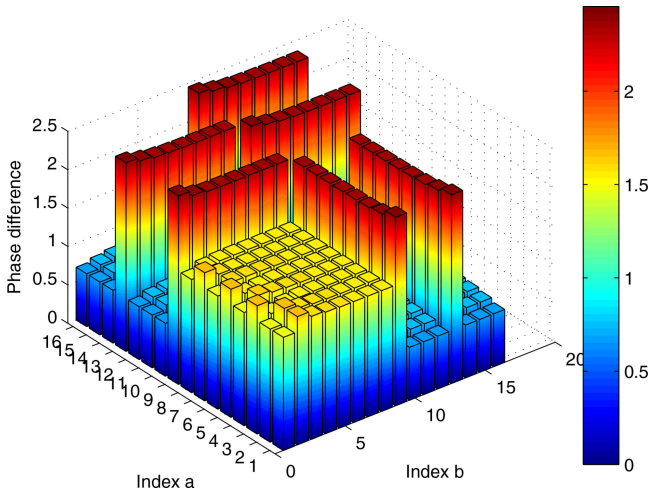

Fig. 13. Phase difference of HRCI code with $N = 16, M = 8$.

differences between the adjacent elements of the DRCI coding matrix, the HRCI coding matrix and IFFT transformation matrix in Fig. 12–Fig. 14. Comparing Fig. 12–Fig. 14, we can observe from Fig. 13 that the phase differences between the adjacent elements of the HRCI coding matrices have no zero values, which provides the noise-resistant performance benefits and PAPR reduction to the SOFDM systems.

Moreover, from Fig. 12, we can observe that the phase difference has zero values. It is worth pointing out that the zero values are induced by the zero elements in the matrix $\mathbf{S}$ in equation (46) instead of being the difference between the two adjacent nonzero elements with the same phases. Accordingly, when calculating the minimum phase difference, it's meaningless to evaluate these zero values. Naturally, we obtain from Fig. 12–Fig. 14 that the minimum phase difference between the adjacent elements in the DRCI coding matrix, the HRCI coding matrix and IFFT transformation matrix are 0.68 rad, 0.68 rad and 0, respectively.

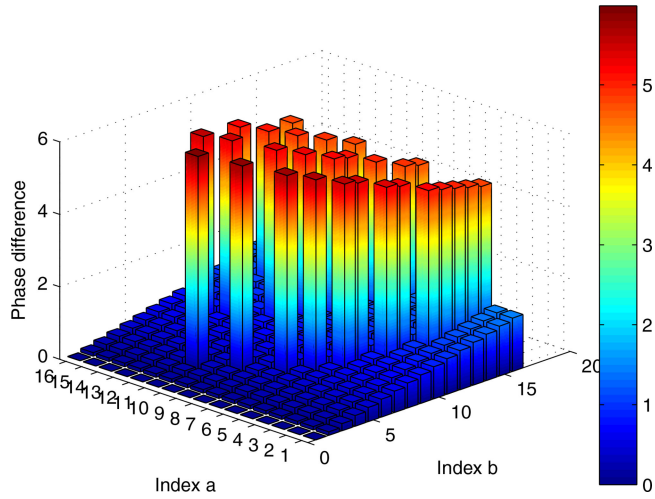

Fig. 14. Phase difference of IFFT with $N = 16$.

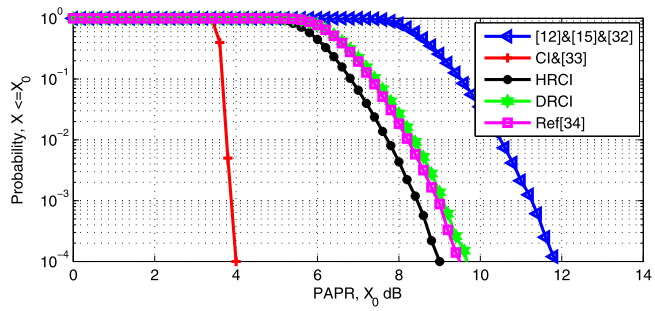

Fig. 15. The PAPR(CCDF) performances of SOFDM systems using CI, HRCI and DRCI codes. $M = 16$. (PAPR:peak-toaverage power ratio; CCDF:complementary cumulative distribution function.).

C. PAPR Performances and Comparisons

Fig. 15 illustrates the PAPR performances of SOFDM systems using 64QAM modulation and employing CI, HRCI and DRCI codes. It can be observed that with the aid of HRCI and DRCI codes, the PAPR performances have been improved about 2dB at possibility of 10^{-4} compared with the system without using spreading code in references [12], [15], [32]. Moreover, the SOFDM systems using recursion-based spreading codes achieve similar performances to the newly proposed PAPR reduction technique by using biased sub-carriers in [34]. When compared with CI coded system and reference [33], HRCI and DRCI coded systems lost about 5dB of PAPR due to the Hadamard and diagonal recursion processes, which is acceptable considering the communication robustness enhancement in Fig. 6. More explicitly, reference [33] is an application of CI code which solves the PAPR issue of DCSK design and has the same PAPR performance as conventional CI code.

Subsequently, we simulate the power of a random symbol of SOFDM systems in Fig. 16. It can be observed that, with the same inputs, the peak values of the symbol power of HRCI and DRCI codes aided SOFDM systems are much lower than those in conventional OFDM systems with the same average symbol power. More explicitly, the PAPR value of this frame of HRCI code, DRCI code and OFDM are 6 dB, 6.23 dB and

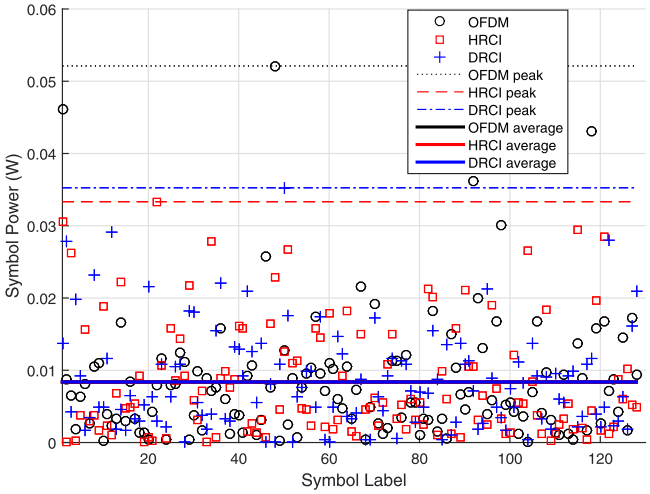

Fig. 16. The power of a random symbol in SOFDM systems using CI, HRCI and DRCI codes. $M = 16$.

7.93 dB respectively, which indicates the HRCI and DRCI coding scheme can provide about a 2 dB PAPR improvement for the same OFDM symbol.

VI. Conclusion

In this paper, we present recursive HRCI and DRCI codes to combat the phase noises and RCFO existed in high speed SOFDM systems. With the aid of recursions, the high order HRCI and DRCI codes can be generated from low order CI codes, thus the phase intervals among the symbols are enlarged and more reliable communication performances than conventional high order one can be attained. We prove that the invertibility properties are held during the recursion procedure, which verifies the feasibility of applying the proposed HRCI codes and DRCI codes in both transmitters and receivers. Then, we analyze the SINR performances of HRCI and DRCI codes aided systems. Simulations are performed to investigate both the BER performances and the PAPR performances for our presented recursion-based transmission scheme design. Numerical results of BER as well as SINR verify that with the aid of HRCI and DRCI codes, the SOFDM systems are less sensitive to phase noises and RCFO, thereby achieving more reliable performances. Moreover, the simulation results also verify the effectiveness of our theoretical SINR analysis, and the PAPR performances are satisfactory compared with the counterpart schemes. Therefore, using the presented HRCI codes and DRCI codes, phase noises are reduced and RCFO is compensated, thus more reliable and more robust transmission capabilities can be achieved by SOFDM systems for the end users.

Appendix

As mentioned in Section IV, in order to evaluate the performances of the SOFDM systems employing the presented HRCI codes and DRCI codes, we here provide details of how to calculate $E[|b_i(q)|^2]$ and $E[|b_d(q)|^2]$ in the SINR evaluation expression given by Eq.(70).

Specifically, utilizing equation (69), $|b_i(q)|^2$ can be calculated by

$$|b_i(q)|^2 = \frac{1}{N^2}\sum_{k=0}^{N-1}\sum_{i=0,i\neq q}^{N-1}\sum_{l=0}^{N-1}\sum_{f=0}^{N-1}\sum_{p=0,p\neq q}^{N-1}\sum_{r=0}^{N-1} a_i a_p^* \mathbf{G}_{i,l}\mathbf{G}_{p,f}^*\mathbf{K}_{k,q}\mathbf{K}_{r,q}^* H'(l)H'^*(f)I(l-k) \cdot I^*(f-r)f_N(\nu_k)f_N^*(\nu_r)e^{j2\pi N_B(k\nu_k - r\nu_r)/N}. \tag{A1}$$

Since the frequency domain channel response $H'(l)$ is independent from phase factor $I(l-k)$ and RCFO factor $e^{j2\pi N_B k\nu_k/N} f_N(\nu_k)$, after applying mean process $E(\cdot)$ to $|b_i(q)|^2$, we have

$$E[|b_i(q)|^2] = \frac{1}{N^3}\sum_{q=0}^{N-1}\sum_{k=0}^{N-1}\sum_{i=0,i\neq q}^{N-1}\sum_{l=0}^{N-1}\sum_{f=0}^{N-1}\sum_{p=0,p\neq q}^{N-1}\sum_{r=0}^{N-1} a_i a_p^* \mathbf{G}_{i,l}\mathbf{G}_{p,f}^*\mathbf{K}_{k,q}\mathbf{K}_{r,q}^* H'(l)H'^*(f) \times E[I(l-k)I^*(f-r)] \cdot f_N(\nu_k)f_N^*(\nu_r)e^{j2\pi N_B(k\nu_k - r\nu_r)/N}. \tag{A2}$$

With the aid of equation (10), $E[e^{j\delta}]$ is calculated as

$$E[e^{j\delta}] = \int_{-\infty}^{+\infty} e^{j\delta}p(\delta)d\delta = \int_{-\infty}^{+\infty} e^{-j\delta t}p(\delta)d\delta|_{t=-1} = \frac{1}{\sqrt{2\pi}\sigma_\delta}\sqrt{2\pi\sigma_\delta^2}e^{-\frac{\sigma_\delta^2 t^2}{2}}|_{t=-1}| = e^{-\frac{\sigma_\delta^2}{2}}, \tag{A3}$$

where $\delta \sim N(0,\sigma_\delta^2)$ and $p(\delta) = \frac{1}{\sqrt{2\pi}\sigma_\delta}e^{-\frac{\delta^2}{2\sigma_\delta^2}}$. Moreover, the expression of $E[I(s)I^*(w)]$ is

$$I(s)I^*(w) = \frac{1}{N^2}\sum_{n=0}^{N-1}\sum_{t=0}^{N-1} e^{j\frac{2\pi sn}{N}+j\phi_n}e^{-j\frac{2\pi wt}{N}-j\phi_t} = \frac{1}{N^2}\sum_{n=0}^{N-1}\sum_{t=0}^{N-1} e^{j\frac{2\pi}{N}(sn-wt)}e^{j(\phi_n-\phi_t)}$$

$$E[I(s)I^*(w)] = \frac{1}{N^2}\sum_{n=0}^{N-1}\sum_{t=0}^{N-1} e^{j\frac{2\pi}{N}(sn-wt)}e^{-\frac{\sigma_\delta^2}{2}|n-t|}. \tag{A4}$$

The expression of $E[I(l-k)I^*(f-r)]$ is obtained by replacing s with $l-k$ and w with $f-r$ in (A4) as

$$E[I(l-k)I^*(f-r)] = \frac{1}{N^2}\sum_{n=0}^{N-1}\sum_{t=0}^{N-1} e^{j\frac{2\pi}{N}(ln+rt-kn-ft)} \times e^{-\frac{\sigma_\delta^2}{2}|n-t|}. \tag{A5}$$

Thus, the expression of $E[|b_i(q)|^2]$ is

$$E[|b_i(q)|^2] = \frac{1}{N^3}\sum_{q=0}^{N-1}\sum_{k=0}^{N-1}\sum_{i=0,i\neq q}^{N-1}\sum_{l=0}^{N-1}\sum_{f=0}^{N-1}\sum_{p=0,p\neq q}^{N-1}\sum_{r=0}^{N-1} a_i a_p^* \mathbf{G}_{i,l}\mathbf{G}_{p,f}^*\mathbf{K}_{k,q}\mathbf{K}_{r,q}^* H'(l)H'^*(f) \times e^{j\frac{2\pi}{N}(ln+rt-kn-ft)} \cdot e^{-\frac{\sigma_\delta^2}{2}|n-t|} f_N(\nu_k) f_N^*(\nu_r) e^{j2\pi N_B(k\nu_k - r\nu_r)/N}. \tag{A6}$$

Similarly, the expression of $E[|b_d(q)|^2]$ is obtained as

$$E[|b_d(q)|^2] = \frac{1}{N^5}\sum_{q=0}^{N-1}\sum_{k=0}^{N-1}\sum_{l=0}^{N-1}\sum_{f=0}^{N-1}\sum_{r=0}^{N-1}\sum_{n=0}^{N-1}\sum_{t=0}^{N-1} |a_q|^2 \mathbf{G}_{q,l}\mathbf{G}_{q,f}^*\mathbf{K}_{k,q}\mathbf{K}_{r,q}^* H'(l)H'^*(f) \times e^{j\frac{2\pi}{N}(ln+rt-kn-ft)} \cdot e^{-\frac{\sigma_\delta^2}{2}|n-t|} f_N(\nu_k) f_N^*(\nu_r) e^{j2\pi N_B(k\nu_k - r\nu_r)/N}. \tag{A7}$$

ACKNOWLEDGMENT

The authors thank the editor and all the reviewers' for their precious time and helpful comments. H. Lu would like to thank A. Li's remarkable contribution in derivation of the expression of SINR, and also like to thank the invaluable support from Y. Liao.

REFERENCES

[1] G. Saulnier, Z. Ye, and M. Medley, "Performance of a spread spectrum OFDM system in a dispersive fading channel with interference," in *Proc. IEEE Mil. Commun. Conf.*, Oct. 1998, vol. 2, pp. 679–683.

[2] H. G. Myung, J. Lim, and D. J. Goodman, "Peak-to average power ratio of single carrier FDMA signals with pulse shaping," in *Proc. IEEE 17th Int. Symp. Pers., Indoor Mobile Radio Commun.*, Sep. 2006, pp. 1–5.

[3] G. Berardinelli, F. Tavares, T. B. Sorensen, P. Mogensen, and K. Pajukoski, "Zero-tail DFT-spread-OFDM signals," in *Proc.IEEE Globecom Workshops*, 2013, pp. 229–234.

[4] A. Sahin, R. Yang, M. Ghosh, and R. L. Olesen, "An improved unique word DFT-Spread-OFDM scheme for 5G systems," in *Proc. IEEE Globecom Workshops*, Dec. 2015, pp. 1–6.

[5] G. Berardinelli, K. I. Pedersen, T. B. Sorensen, and P. Mogensen, "Generalized DFT-Spread-OFDM as 5G waveform," *IEEE Commun. Mag.*, vol. 54, no. 11, pp. 99–105, Nov. 2016.

[6] X. Li, V. Chakravarthy, B. Wang, and Z. Wu, "Spreading code design of adaptive non-contiguous SOFDM for dynamic spectrum access," *IEEE J. Sel. Topics Signal Process.*, vol. 5, no. 1, pp. 190–196, Feb. 2011.

[7] D. Wiegandt, Z. Wu, and C. Nassar, "High capacity, high performance, low PAPR OFDM via carrier interferometry," *IEEE Trans. Commun.*, vol. 51, no. 7, pp. 1123–1134, Jul. 2003.

[8] Z. Wu and C. Nassar, "Narrowband interference rejection in OFDM via carrier interferometry spreading codes," *IEEE Trans. Wireless Commun.*, vol. 4, no. 4, pp. 1491–1505, Jul. 2005.

[9] T. Pollet, M. van Bladel, and M. Moeneclaey, "BER sensitivity of OFDM systems to carrier frequency offset and Wiener phase noise," *IEEE Trans. Commun.*, vol. 43, no. 2–4, pp. 191–193, Feb.–Apr. 1995.

[10] S. Wu and Y. Bar-Ness, "OFDM systems in the presence of phase noise: Consequences and solutions," *IEEE Trans. Commun.*, vol. 52, no. 11, pp. 1988–1996, Nov. 2004.

[11] P. Mathecken, T. Riihonen, S. Werner, and R. Wichman, "Phase noise estimation in OFDM: Utilizing its associated spectral geometry," *IEEE Trans. Signal Process.*, vol. 64, no. 8, pp. 1999–2012, Apr. 2016.

[12] D. D. Lin, R. Pacheco, T. J. Lim, and D. Hatzinakos, "Joint estimation of channel response, frequency offset, phase noise in OFDM," *IEEE Trans. Signal Process.*, vol. 54, no. 9, pp. 3542–3554, Sep. 2006.

[13] D. D. Lin and T. J. Lim, "The variational inference approach to joint data detection and phase noise estimation in OFDM," *IEEE Trans. Signal Process.*, vol. 55, no. 5, pp. 1862–1874, May 2007.

[14] Y. Chi, A. Gomaa, N. Al-Dhahir, and A. R. Calderbank, "Training signal design and tradeoffs for spectrally-efficient multi-user MIMO OFDM systems," *IEEE Trans. Wireless Commun.*, vol. 10, no. 7, pp. 2234–2245, Jul. 2011.

[15] O. H. Salim, A. A. Nasir, H. Mehrpouyan, W. Xiang, S. Durrani, and R. A. Kennedy, "Channel, phase noise, and frequency offset in OFDM systems: Joint estimation, data detection, and hybrid Cramér-Rao lower bound," *IEEE Trans. Commun.*, vol. 62, no. 9, pp. 3311–3325, Sep. 2014.

[16] M. Morelli, G. Imbarlina, and M. Moretti, "Estimation of residual carrier and sampling frequency offsets in OFDM-SDMA uplink transmissions,"*IEEE Trans. Wireless Commun.*, vol. 9, no. 2, pp. 734–744, Feb. 2010.

[17] C. Oberli, "ML-based tracking algorithms for MIMO-OFDM,"*IEEE Trans. Wireless Commun.*, vol. 6, no. 7, pp. 2630–2639, Jul. 2007.

[18] M. Sliskovic, "Carrier and sampling frequency offset estimation and correction in multicarrier systems," in *Proc. GLOBECOM*, Feb. 2001, vol. 1, pp. 285–289.

[19] K. Shi, E. Serpedin, and P. Ciblat, "Decision-directed fine synchronization in OFDM systems," *IEEE Trans. Commun.*, vol. 53, no. 3, pp. 408–412, Mar. 2005.

[20] H. Lu, L. Zhang, F. Fang, and Z. Wu, "Phase Noise resistant rotation iteration based carrier interferometry code design for high speed optical OFDM systems," *IEEE Commun. Lett.*, vol. 22, no. 3, pp. 522–525, Mar. 2018.

[21] J. Sylvester, "Thoughts on inverse orthogonal matrices, simultaneous sign successions, and tessellated pavements in two or more colours, with applications to Newton's rule, ornamental tile-work, and the theory of numbers," *Philos. Mag.*, vol. 34, no. 232, pp. 461–475, 1867.

[22] R. Rajbanshi, Q. Chen, A. Wyglinski, G. Minden, and J. Evans, "Quantitative comparison of agile modulation technique for cognitive radio transceivers," in *Proc. 4th IEEE Consum. Commun. Netw. Conf.*, Jan. 2007, pp. 1144–1148.

[23] A. Shalom, I. Tselniker, and M. Nazarathy, "Improving the phase noise tolerance of subbanded DFT-spread OFDM by nonredundant interleaving," *J. Lightw. Technol.*, vol. 32, no. 21, pp. 4119–4132, Nov. 2014.

[24] M. S. El-Tanany, Y. Wu, and L. Hazy, "Analytical modeling and simulation of phase noise interference in OFDM-based digital television terrestrial broadcasting systems," *IEEE Trans. Broadcast.*, vol. 47, no. 1, pp. 20–31, Mar. 2001.

[25] A. G. Armada and M. Calvo, "Phase noise and sub-carrier spacing effects on the performance of an OFDM communication system," *IEEE Commun. Lett.*, vol. 2, no. 1, pp. 11–13, Jan. 1998.

[26] A. G. Armada, "Understanding the effects of phase noise in orthogonal frequency division multiplexing (OFDM)," *IEEE Trans. Broadcast.*, vol. 47, no. 2, pp. 153–159, Jun. 2001.

[27] G. J. Foschini and G. Vannucci, "Characterizing filtered light waves corrupted by phase noise," *IEEE Trans. Inf. Theory*, vol. 34, no. 6, pp. 1437–1448, Nov. 1988.

[28] A. Demir, A. Mehrotra, and J. Roychowdhury, "Phase noise in oscillators: A unifying theory and numerical methods for characterization," *IEEE Trans. Circuits Syst.*, vol. 47, no. 5, pp. 655–674, May 2000.

[29] M. Morelli and U. Mengali, "Carrier-frequency estimation for transmission over selective channels," *IEEE Trans. Commun.*, vol. 48, no. 9, pp. 1580–1589, Sep. 2000.

[30] P. C. Weeraddana, N. Rajatheva, and H. Minn, "Probability of error analysis of BPSK OFDM systems with random residual frequency offset," *IEEE Trans. Commun.*, vol. 57, no. 1, pp. 106–116, Jan. 2009.

[31] R. Bellman, *Introduction To Matrix Analysis*. New York, NY, USA: McGraw-Hill, 1960, ch. 20.

[32] P. Rabiei, W. Namgoong, and N. Al-Dhahir, "A non-iterative technique for phase noise ICI mitigation in packet-based OFDM systems," *IEEE Trans. Signal Process.*, vol. 58, no. 11, pp. 5945–5950, Nov. 2010.

[33] Z. Liu, L. Zhang, and Z. Chen, "Low PAPR OFDM-based DCSK design with carrier interferometry spreading codes," *IEEE Commun. Lett.*, vol. 22, no. 8, pp. 1588–1591, Aug. 2018.

[34] M. A. Khan and R. K. Rao, "Low-complexity PAPR reduction technique for OFDM systems using biased subcarriers," *Can. J. Elect. Comput. Eng.*, vol. 39, pp. 19–25, Nov. 2016.

Huaiyin Lu received the B.S. degree in electronic information science and technology in 2015 from Sun Yat-sen University, Guangzhou, China, where he is currently working toward the Ph.D. degree in information and communication engineering. His research interests include cognitive radio networks, chaotic communications, visible light communications, 5G technology, and machine learning.

Lin Zhang (M'03–SM'07) received the B.S. and M.S. degrees in electrical engineering from Shanghai University, Shanghai, China, in 1997 and 2000, respectively, and the Ph.D. degree in electrical engineering from Sun Yat-sen University, Guangzhou, China, in 2003. She was with the Department of Electrical Engineering, Sun Yat-sen University in 2003 and has served as an Associate Professor in 2007. From 2008 to 2009, she was a Visiting Researcher with the Electrical and Computer Engineering Department, University of Maryland, College Park, MD, USA. Her research has been supported by the National Natural Science Foundation of China, Guangdong Provincial Key Laboratory of Information Security Technology, the Science and Technology Program Project of Guangdong Province. Her current research interests are in the area of signal processing and their applications to wireless communication systems.

Xianyu Chen received the B.Eng. degree in communication engineering and the M.Eng. degree in information and communication engineering from Sun Yet-sen University, Guangzhou, China, in 2015 and 2018, respectively. His research interests include computer vision, machine learning, convex optimization, and estimation theory.

Zhiqiang Wu (M'02–SM'17) received the B.S. degree in electrical engineering from the Beijing University of Posts and Telecommunications, Beijing, China, in 1993, the M.S. degree in electrical engineering from Peking University, Beijing, China, in 1996, and the Ph.D. degree in electrical engineering from Colorado State University, Fort Collins, CO, USA, in 2002. He served as an Assistant Professor with the Department of Electrical and computer Engineering, West Virginia University Institute of Technology from 2003 to 2005. He joined Wright State University, Dayton, OH, USA, in 2005, where he is currently a Full Professor with the Department of Electrical Engineering. His research has been supported by National Science Foundation (NSF), Air Force Research Lab (AFRL), Office of Naval Research (ONR), Air Force Office of Scientific Research (AFOSR), and Ohio Federal Research Network (OFRN). He has also held visiting positions with Peking University, Harbin Engineering University, Guizhou Normal University, and Tibet University.